Journal of Molecular and Cellular Cardiology 52 (2012) 1122–1134

Contents lists available at SciVerse ScienceDirect

Journal of Molecular and Cellular Cardiology

journal homepage: www.elsevier.com/locate/yjmcc

Original article

The natriuretic peptides BNP and CNP increase heart rate and electrical conduction by stimulating ionic currents in the sinoatrial node and atrial myocardium following activation of guanylyl cyclase-linked natriuretic peptide receptors

Jeremy Springer, John Azer, Rui Hua, Courtney Robbins, Andrew Adamczyk, Sarah McBoyle, Mary Beth Bissell, Robert A. Rose *

Department of Physiology and Biophysics, Faculty of Medicine, Dalhousie University, Halifax, Nova Scotia, Canada

ARTICLE INFO

Article history:
Received 26 November 2011
Received in revised form 16 December 2011
Accepted 24 January 2012
Available online 1 February 2012

Keywords:
Natriuretic peptides
Natriuretic peptide receptors
Electrocardiography
Sinoatrial node
Action potential
Ion channels
Phosphodiesterase

ABSTRACT

Natriuretic peptides (NPs) are best known for their ability to regulate blood vessel tone and kidney function whereas their electrophysiological effects on the heart are less clear. Here, we measured the effects of BNP and CNP on sinoatrial node (SAN) and atrial electrophysiology in isolated hearts as well as isolated SAN and right atrial myocytes from mice. BNP and CNP dose-dependently increased heart rate and conduction through the heart as indicated by reductions in R–R interval, P wave duration and P–R interval on ECGs. In conjunction with these ECG changes BNP and CNP (100 nM) increased spontaneous action potential frequency in isolated SAN myocytes by increasing L-type Ca^{2+} current ($I_{Ca,L}$) and the hyperpolarization-activated current (I_f). BNP had no effect on right atrial myocyte APs in basal conditions; however, in the presence of isoproterenol (10 nM), BNP increased atrial AP duration and $I_{Ca,L}$. Quantitative gene expression and immunocytochemistry data show that all three NP receptors (NPR-A, NPR-B and NPR-C) are expressed in the SAN and atrium. The effects of BNP and CNP on SAN and right atrial myocytes were maintained in mutant mice lacking functional NPR-C receptors and blocked by the NPR-A antagonist A71915 indicating that BNP and CNP function through their guanylyl cyclase-linked receptors. Our data also show that the effects of BNP and CNP are completely absent in the presence of the phosphodiesterase 3 inhibitor milrinone. Based on these data we conclude that NPs can increase heart rate and electrical conduction by activating the guanylyl cyclase-linked NPR-A and NPR-B receptors and inhibiting PDE3 activity.

1. Introduction

Natriuretic peptides (NPs) constitute a family of hormones that have a number of important effects in the cardiovascular system [1,2]. This family includes atrial (ANP), B-type (BNP) and C-type (CNP) NPs, which elicit their physiological effects by binding to specific NP receptors (NPRs) denoted NPR-A, NPR-B and NPR-C [2,3]. NPR-A (which binds ANP and BNP) and NPR-B (which only binds CNP) are particulate guanylyl cyclase (GC) receptors that increase intracellular cGMP upon agonist binding. The cGMP produced downstream of NPR-A/B can modulate several targets including protein kinase G (PKG) and phosphodiesterases 2 and 3 (PDE2 and PDE3) [2,4]. NPR-C, which binds all NPs, is not directly linked to a GC enzyme, but rather is coupled to the activation of inhibitory G proteins (G_i) [5,6].

NPs are powerful regulators of the cardiovascular system and are best known for their ability to regulate intravascular volume and arterial pressure through their effects in the kidneys (natriuresis, diuresis) and on vascular tone [2,7]. In this way NPs can importantly regulate cardiac output by affecting loading conditions on the heart. In contrast, the direct effects of NPs on ion channel function in the myocardium, particularly within the sinoatrial node (SAN), are much less well understood. Synthetic natriuretic peptides are in use [8] or in development [9] for the treatment of heart failure, thus it is essential to understand how these hormones directly modulate cardiac function.

Recently we demonstrated that CNP can slow heart rate (HR) by decreasing L-type Ca^{2+} current ($I_{Ca,L}$) in isolated SAN myocytes [10,11]. These effects were shown to be dependent on activation of NPR-C and were only seen in the presence of a saturating dose (1 μM) of the β-adrenergic receptor (β-AR) agonist isoproterenol (ISO). On the other hand some studies have shown that NPs can increase HR and/or SAN activity *in vivo* and/or in isolated atrial preparations [12–14]. These variable responses may be related to a lack of understanding of how different NPRs contribute to physiological responses in different conditions. Given that HR is a critical determinant of cardiac

* Corresponding author at: Department of Physiology and Biophysics, Dalhousie University, Sir Charles Tupper Medical Building, Room 3F, 5850 College Street, Halifax, Nova Scotia, Canada, B3H 4R2. Tel.: +1 902 494 2268; fax: +1 902 494 1685.
E-mail address: robert.rose@dal.ca (R.A. Rose).

0022-2828/$ – see front matter © 2012 Elsevier Ltd. All rights reserved.
doi:10.1016/j.yjmcc.2012.01.018

output there is clearly a need to better understand how NPs affect cardiac chronotropy.

HR is determined intrinsically by the rhythmic spontaneous activity of specialized pacemaker myocytes in the SAN [15–18]. Critical to pacemaker activity, the SAN myocyte gradually depolarizes during the diastolic period until the threshold for the next AP is reached. This gradual depolarization is called the diastolic depolarization (DD) and is the fundamental feature of the SAN myocyte that enables pacemaker activity. Several ionic mechanisms have been shown to play a role in the generation of the DD. These include, among others, the hyperpolarization-activated current (I_f) carried by HCN channels, T- and L-type Ca^{2+} currents ($I_{Ca,T}$ and $I_{Ca,L}$), a delayed rectifier K^+ current (I_{Kr}) and an inward Na^+–Ca^{2+} exchange current (I_{NCX}) driven by the release of Ca^{2+} from the sarcoplasmic reticulum (SR) [17,18]. Atrial myocytes, on the other hand, do not display spontaneous APs. Instead they are stimulated to fire APs from a stable resting membrane potential when spontaneously generated APs exit the SAN and depolarize the surrounding atrial myocardium.

The purpose of this study was to determine the effects of BNP and CNP on HR and electrical conduction in isolated hearts in basal conditions and to determine the molecular mechanism of these effects in isolated SAN and working atrial myocytes. Our studies provide new insight into the mechanisms by which NPs regulate pacemaker activity and chronotropic responses in the heart. By using BNP and CNP as agonists we were able to assess the role of all three NPRs in these effects.

2. Materials and methods

An expanded Methods section is available in the Online Supplement.

2.1. Animals

This study utilized male wildtype C57Bl/6 mice (Charles River) and mutant mice lacking functional NPR-C receptors (NPR-$C^{-/-}$; The Jackson Laboratory) [19] between the ages 10 and 14 weeks. Experimental procedures were in accordance with the regulations of The Canadian Council on Animal Care and were approved by Dalhousie University.

2.2. Experimental approaches

Experimental approaches included ECG recordings in Langendorff-perfused hearts [10,20], action potential (AP) and ionic current measurements on isolated SAN and atrial myocytes using the patch-clamp technique [21], gene expression analysis in SAN and right atrial tissue using quantitative PCR [22], and immunocytochemistry on isolated SAN and atrial myocytes [23].

2.3. Statistical analysis

All summary data are presented as means ± SEM. Data were analyzed using a paired Student's *t*-test, or one-way/two-way ANOVAs with Tukey's or Student–Newman–Keuls' posthoc analysis. $P<0.05$ was considered significant.

3. Results

3.1. Effects of BNP and CNP on HR and electrical conduction

Initial experiments measured the effects of BNP and CNP on HR and electrical conduction by measuring ECGs in Langendorff-perfused mouse hearts. Representative ECG recordings (Figs. 1A and B) and time course experiments (Figs. 1C and D) demonstrate that BNP and CNP (500 nM) rapidly and reversibly increased HR. To assess the dose dependence of these effects BNP and CNP were applied at doses ranging from 1 nM to 1000 nM (Figs. 1E and F). BNP significantly increased HR at all doses except the lowest (1 nM) dose. The EC_{50} values for BNP and CNP were 304 ± 42 nM and 319 ± 49 nM respectively.

BNP and CNP also increased conduction across the atria and through the atrioventricular (AV) node, as indicated by P wave duration and PR interval analysis (Supplemental Table 1). Application of BNP (500 nM) shortened ($P<0.05$) the P wave duration from 9.8 ± 0.7 ms to 8.3 ± 1.3 ms and the PR interval from 51.7 ± 3.1 to 37.8 ± 0.9 ms while CNP (500 nM) shortened ($P<0.05$) the P wave duration from 10.4 ± 0.6 to 8.3 ± 0.3 and the PR interval from 39.2 ± 2.6 to 28.2 ± 1.1 ms. The effects of BNP and CNP on ECG parameters were also dose dependent (not shown).

3.2. Effects of BNP and CNP on isolated SAN myocyte spontaneous APs

The ability of NPs to increase HR in isolated hearts is indicative of intrinsic effects on the SAN; therefore, spontaneous APs were measured in isolated SAN myocytes during acute application of NPs. Consistent with the isolated heart experiments, BNP and CNP (100 nM) increased spontaneous AP frequency (Figs. 2A and B) in SAN myocytes. On average BNP increased ($P<0.05$) SAN myocyte AP frequency (Fig. 2C) from 148.5 ± 5.5 to 180 ± 4.5 APs/min in association with an increase ($P<0.05$) in the slope of the DD (Fig. 2D) from 31 ± 1.7 to 48.3 ± 1.3 mV/s. BNP had no effect ($P=0.88$) on the MDP (−66.3 ± 0.9 mV in control vs. −66.3 ± 0.7 mV in BNP; Fig. 2E). CNP increased ($P<0.05$) spontaneous AP frequency (Fig. 2F) from 140.5 ± 12.2 to 167.5 ± 13 APs/min. Application of CNP also increased ($P<0.05$) the DD slope (Fig. 2G) from 25.8 ± 4.6 to 43.1 ± 7.2 mV/s without changing ($P=0.72$) the MDP (−65.3 ± 2 in control vs. −65.5 ± 2.4; Fig. 2H). Analysis of additional spontaneous AP parameters is presented in Supplemental Tables 2 and 3. These data show that BNP and CNP also prolonged ($P<0.05$) APD_{50} from 48.3 ± 4.8 to 54.3 ± 4.1 ms and 40.6 ± 3.6 to 48.5 ± 4.4 ms, respectively. BNP and CNP did not significantly alter AP upstroke velocity (V_{max}) or the AP overshoot (OS).

3.3. Effects of BNP and CNP on ionic currents in isolated SAN myocytes

We next tested the effects of BNP and CNP on ionic currents known to contribute prominently to the DD phase of the AP in SAN myocytes including $I_{Ca,L}$ and the hyperpolarization-activated current I_f [15,16,18]. $I_{Ca,L}$ in SAN myocytes is dependent on both $Ca_V1.2$ and $Ca_V1.3$ channels [24,25] and we used voltage clamp protocols that measure the contribution of both Ca^{2+} channel isoforms to $I_{Ca,L}$ (see supplemental methods) [21,24,26]. Summary current–voltage (I–V) relationships illustrate that BNP (100 nM; Fig. 3C) increased ($P<0.05$) peak $I_{Ca,L}$ from –4.4 ± 0.6 to −6.1 ± 0.5 pA/pF while CNP (100 nM; Fig. 3D) increased ($P<0.05$) peak $I_{Ca,L}$ from −4.3 ± 0.3 to −5.9 ± 0.3 pA/pF. The effects of NPs on SAN myocyte $I_{Ca,L}$ were further studied by performing steady state conductance analysis. BNP increased ($P<0.05$) maximum $I_{Ca,L}$ conductance (G_{max}) from 127.7 ± 5.1 to 148.6 ± 2.4 pS/pF and shifted the $V_{1/2(act)}$ from −17.7 ± 1.9 to −20.8 ± 0.8 mV (Fig. 3E). CNP increased ($P<0.05$) $I_{Ca,L}$ G_{max} from 117 ± 3.7 to 160.2 ± 2.2 pS/pF while shifting the $V_{1/2(act)}$ from −16.4 ± 1.4 to −19.1 ± 0.6 mV (Fig. 3F).

We next measured the effects of NPs on I_f. Representative I_f recordings (measured during 2 s voltage clamp steps to −120 mV; Figs. 4A and B) and summary I−V relationships (measured as the peak current density at the end of 2 s voltage clamp steps between −30 and −160 mV; Figs. 4C and D) demonstrate that BNP and CNP (100 nM) similarly increased ($P<0.05$) I_f density. In association with these increases in I_f density BNP and CNP shifted ($P<0.05$) the $V_{1/2(act)}$ from −112.4 ± 2.3 to −99.3 ± 0.9 mV and −109.4 ± 1.9 to −101.6 ± 1.4 mV, respectively (Figs. 4E and F). The slope factor (k) was not altered by BNP and CNP ($P=0.189$).

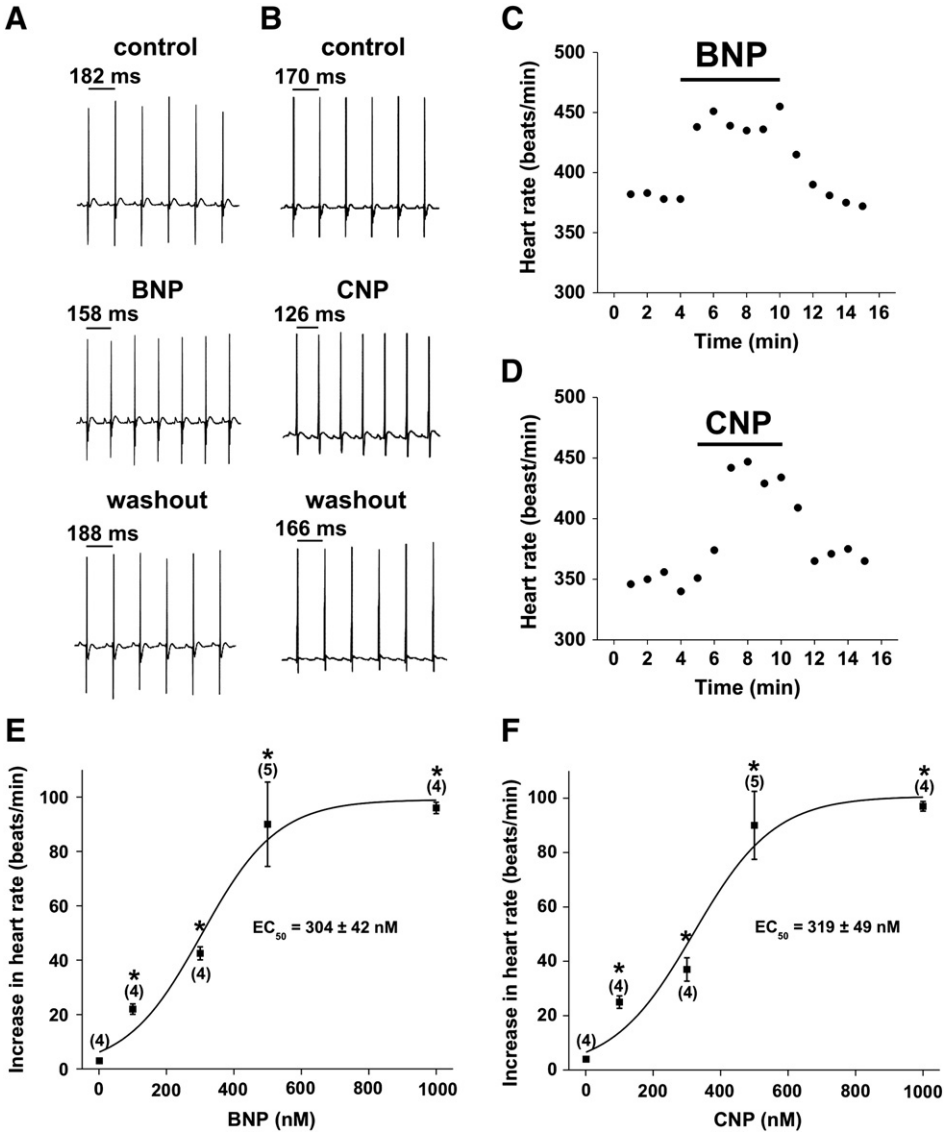

Fig. 1. Effects of BNP and CNP on HR in Langendorff-perfused mouse hearts. (A and B) Representative ECG recordings (1 s duration) in control conditions, following the application of BNP or CNP (500 nM), and after peptide wash off. (C and D) Time course of the effects of BNP and CNP (500 nM) on HR. (E and F) Summary dose–response curves for the effects of BNP and CNP (1 nM–1000 nM) on HR. $n = 4$–5 hearts for each peptide at each concentration; $^*P<0.05$ by one-way ANOVA with a Tukey posthoc test. See Supplemental Table 1 for analysis of additional ECG parameters.

3.4. Effects of BNP on right atrial myocytes

Based on our ECG data showing changes in atrial conduction we also measured the effects of BNP (100 nM) on APs and $I_{Ca,L}$ in right atrial myocytes. In contrast to SAN myocytes, BNP had no effect on right atrial myocyte APs in basal conditions (Fig. 5A). Summary data in Fig. 5C demonstrate that neither AP duration (APD) at 50% repolarization (APD_{50}; 7.4 ± 1.1 ms in control vs. 7.3 ± 1.1 ms in BNP; $P = 0.23$) or 90% repolarization (APD_{90}; 36.3 ± 7.7 ms in control vs. 35.7 ± 7.7 ms in BNP; $P = 0.73$) were changed in the presence of BNP.

We then tested the effects of BNP on atrial APs in the presence of a submaximal dose of the β-AR agonist isoproterenol (ISO; 10 nM). Unlike in basal condition, application of BNP (100 nM) in the presence of ISO prolonged APD (Fig. 5B). As illustrated in Fig. 5D ISO and BNP each progressively increased ($P<0.05$) APD_{50} (13.6 ± 0.8 ms in control, 25.2 ± 1.8 ms in ISO, 31.2 ± 2.2 ms in ISO + BNP) and APD_{70} (23.7 ± 0.7 ms in control, 43.3 ± 2 ms in ISO, 51.3 ± 2.6 ms in ISO + BNP). APD_{90} was increased by ISO ($P<0.05$) and although BNP tended to further prolong APD_{90} this did not reach statistical significance ($P = 0.23$; Fig. 5D).

In association with the prolongation of the AP, BNP (100 nM) also increased right atrial $I_{Ca,L}$ in the presence of ISO (10 nM; Figs. 5E and F). Once again, atrial $I_{Ca,L}$ was recorded from a holding potential of −60 mV in order to record $Ca_V1.2$ and $Ca_V1.3$-dependent $I_{Ca,L}$ [27]. On average, peak atrial $I_{Ca,L}$ was increased ($P<0.05$) from −3.5 ± 0.2 to −9.7 ± 0.7 pA/pF in ISO. Application of BNP in the presence of ISO further increased ($P<0.05$) $I_{Ca,L}$ to −11.7 ± 0.7 pA/pF. Steady state $I_{Ca,L}$ conductance analysis (Fig. 5G) demonstrates that ISO

Fig. 2. Effects of BNP and CNP on spontaneous action potential firing in isolated sinoatrial node myocytes. (A and B) Representative spontaneous AP recordings (5 s duration) in control conditions, following application of BNP or CNP (100 nM) and after peptide wash off. Dotted lines are at 0 mV. Two consecutive APs in control conditions and after application of BNP or CNP are also illustrated in panels A and B (bottom). Summary bar graphs illustrating the effects of BNP and CNP (100 nM) on spontaneous AP frequency (C and F), slope of the diastolic depolarization (D and G) and maximum diastolic potential (E and H). $n = 8$ SAN myocytes for each peptide; $P<0.05$ vs. control by one-way ANOVA with a Tukey posthoc test.

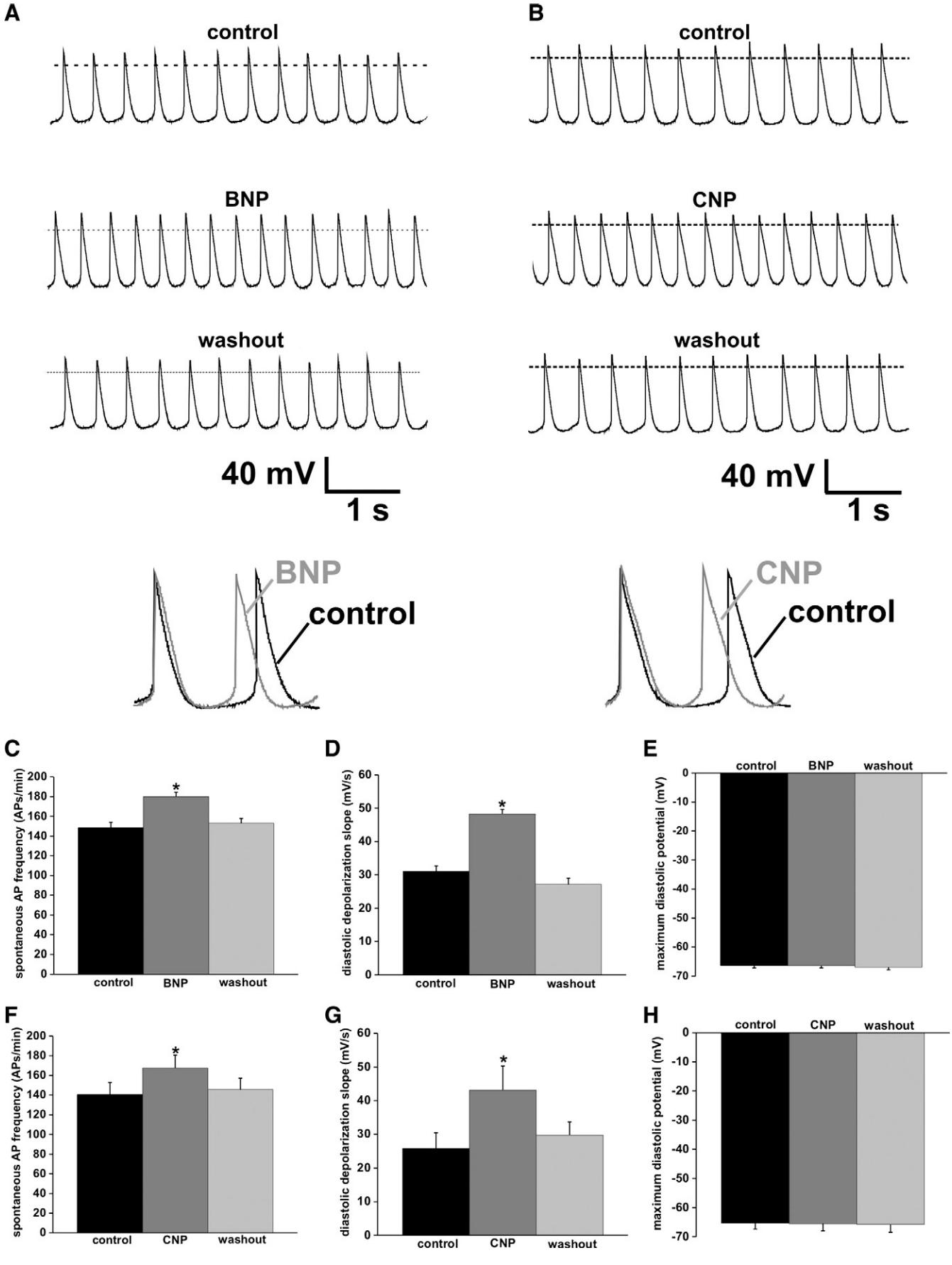
A
control
BNP
washout
40 mV
1 s
B
control
CNP
washout
40 mV
1 s
BNP
control
CNP
control
C
spontaneous AP frequency (APs/min)
control
BNP
washout
D
diastolic depolarization slope (mV/s)
control
BNP
washout
E
maximum diastolic potential (mV)
control
BNP
washout
F
spontaneous AP frequency (APs/min)
control
CNP
washout
G
diastolic depolarization slope (mV/s)
control
CNP
washout
H
maximum diastolic potential (mV)
control
CNP
washout

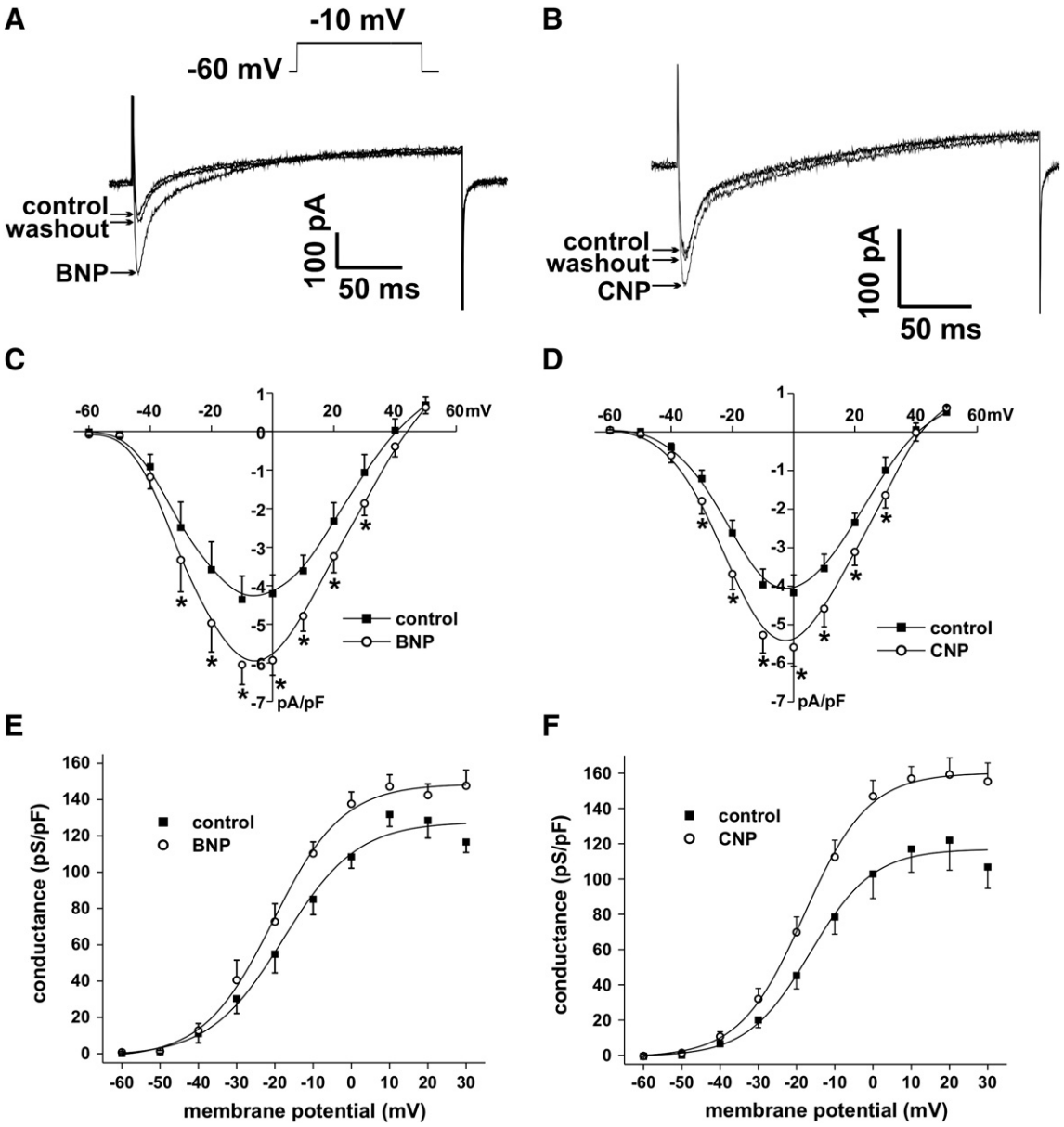

Fig. 3. Effects of BNP and CNP on L-type Ca^{2+} current ($I_{Ca,L}$) in isolated sinoatrial node myocytes. (A and B) Representative $I_{Ca,L}$ recordings in control conditions, following the application of BNP or CNP (100 nM) and after peptide wash off. The voltage clamp protocol used (inset) allows measurement of $Ca_V1.2$ and $Ca_V1.3$ dependent $I_{Ca,L}$ (see Materials and methods). (C and D) Summary I–V relationships for the effects of BNP and CNP (100 nM) on SAN myocyte $I_{Ca,L}$. (E and F) Summary $I_{Ca,L}$ conductance density plots for BNP and CNP (100 nM). See Section 3.3 for details. $n=6$ SAN myocytes for each peptide; $P<0.05$ vs. control by paired Student's *t*-test at each membrane potential.

increased ($P<0.05$) G_{max} from 101.6 ± 5 to 200.1 ± 17 pS/pF and shifted ($P<0.05$) the $V_{1/2(act)}$ from -8.3 ± 0.9 to -13.8 ± 1.2 mV. Application of BNP in the presence of ISO further increased ($P<0.05$) G_{max} to 239.1 ± 16 and hyperpolarized the $V_{1/2(act)}$ to -14.9 ± 1.4 mV. The time course of the effects of ISO and BNP on atrial $I_{Ca,L}$ is presented in Supplemental Fig. 3.

3.5. Expression of natriuretic peptide receptors in the SAN and right atrium

In order to determine the molecular mechanism for the effects of NPs on SAN and atrial myocyte electrophysiology mRNA expression for each NPR was measured in SAN and right atrial tissue samples using quantitative PCR. Glyceraldehyde 3-phosphate dehydrogenase (GAPDH) was used as a reference gene. Samples were confirmed to be from the appropriate region of the myocardium based on the high expression of HCN4 and low expression of ANP in the SAN compared to the atrium (Supplemental Fig. 1A) as described previously [22]. Supplemental Fig. 1B demonstrates that mRNA for Npr1, Npr2 and Npr3 (the genes corresponding to NPR-A, NPR-B and NPR-C) are all present in the SAN and atrial myocardium. Npr1 was more highly ($P<0.05$) expressed in SAN compared to right atrium, whereas Npr3 was more highly expressed ($P<0.001$) in the right atrium compared to the SAN. Npr2 expression did not differ ($P=0.06$) between SAN and right atrial samples. These data further demonstrate that within the SAN Npr1 was more highly expressed than Npr2 ($P<0.05$) and that within the right atrium Npr3 was more highly expressed ($P<0.001$) than Npr1 and Npr2.

Immunocytochemistry using specific antibodies was performed to confirm that NPR proteins were expressed specifically in isolated SAN and right atrial myocytes. Supplemental Fig. 2 demonstrates that spindle shaped myocytes isolated from the SAN stained positively for HCN4 while working myocytes from the right atrial appendage stained positively for ANP as expected [23]. In agreement

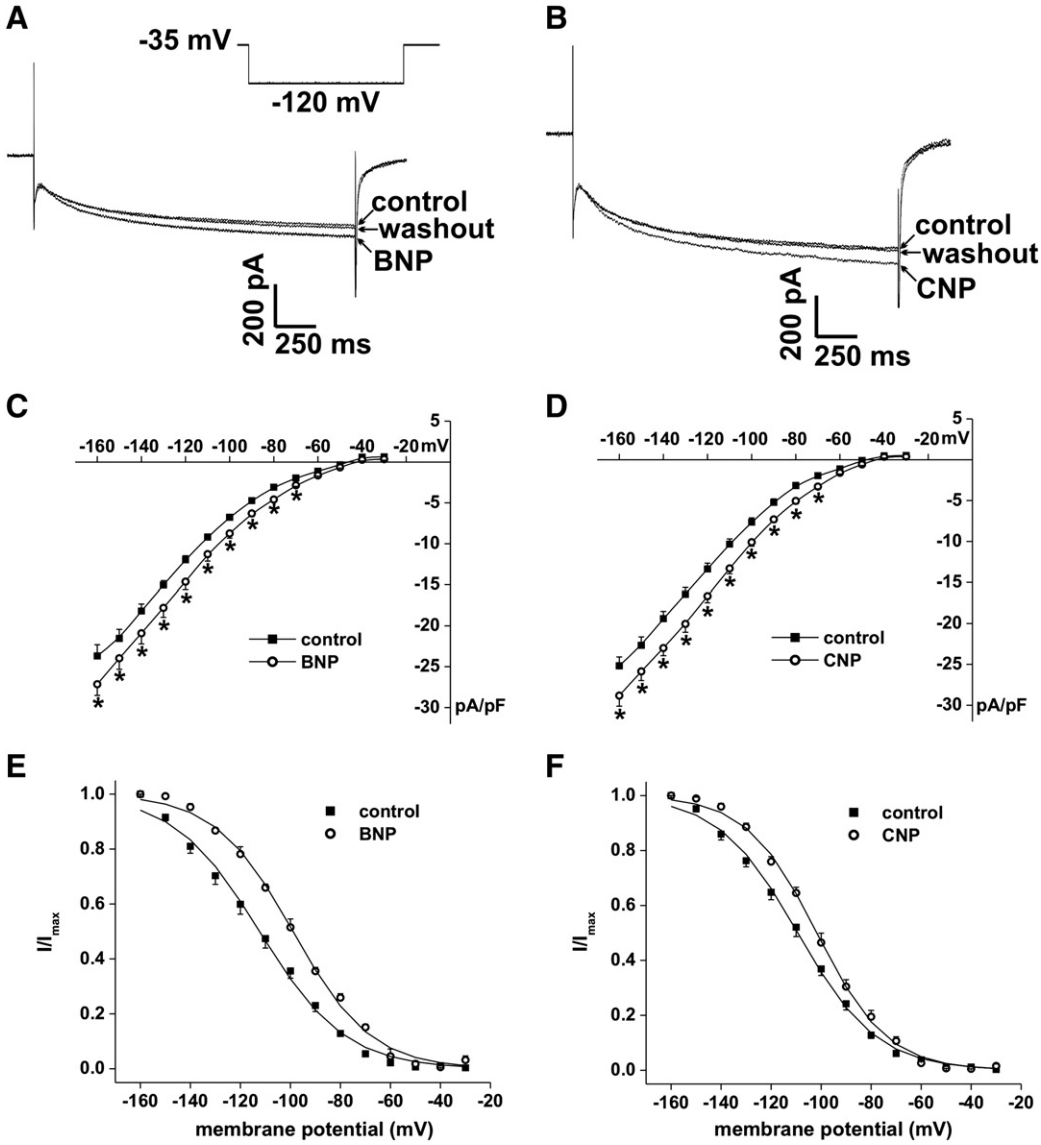

Fig. 4. Effects of BNP and CNP on the hyperpolarization-activated current (I_f) in isolated sinoatrial node myocytes. (A and B) Representative I_f recordings at −120 mV (inset) in control conditions, following the application of BNP or CNP (100 nM) and after peptide wash off. (C and D) Summary I–V relationships for the effects of BNP and CNP (100 nM) on I_f. (E and F) I_f activation curves in control conditions and following the application of BNP or CNP. See Section 3.3 for details. $n=8$ SAN myocytes in the BNP group and 9 SAN myocytes in the CNP group; $P<0.05$ vs. control by paired Student's *t*-test at each membrane potential.

with the qPCR data described above, SAN and right atrial myocytes from the same isolations also stained positively for NPR-A, NPR-B and NPR-C.

3.6. Effects of BNP and CNP in NPR-C$^{-/-}$ mice

The ability of BNP and CNP to increase $I_{Ca,L}$ in SAN and atrial myocytes was somewhat surprising because we have previously demonstrated that CNP can decrease $I_{Ca,L}$ (prestimulated with a maximal 1 μM dose of ISO) by activating NPR-C [10,11,28]. To evaluate the role of NPR-C in the present experimental conditions we used mutant mice lacking functional NPR-C receptors (NPR-C$^{-/-}$). Application of BNP (100 nM) increased spontaneous AP frequency in SAN myocytes from NPR-C$^{-/-}$ mice to a similar extent as wildtype mice (Fig. 6A). On average, BNP increased ($P<0.05$) AP frequency from 147 ± 11.3 to 175 ± 11.4 APs/min in association with an increase ($P<0.05$) in the DD slope (Figs. 6B and C) and APD_{50} (Supplemental Table 2). CNP had comparable effects to BNP whereby spontaneous AP frequency was increased ($P<0.05$) in NPR-C$^{-/-}$ myocytes from 152 ± 9.3 to 184 ± 10.5 APs/min along with increases ($P<0.05$) in DD slope and APD_{50} (Figs. 6D and E; Supplemental Table 3). Consistent with their effects on AP frequency BNP and CNP (100 nM) increased ($P<0.05$) $I_{Ca,L}$ and I_f in NPR-C$^{-/-}$ SAN myocytes as effectively as in wildtype mice (Fig. 6).

Similar results were obtained in isolated right atrial myocytes from NPR-C$^{-/-}$ mice (Supplemental Fig. 4) whereby BNP (100 nM) still effectively increased $I_{Ca,L}$ in the presence of ISO (10 nM). These data suggest that NPR-C is not responsible for the stimulatory effects of BNP and CNP in the SAN in basal conditions or atrial myocytes in submaximal doses of ISO. In agreement with this conclusion we found that application of the NPR-C selective agonist cANF [10,29] had no effect on isolated hearts (500 nM dose) or SAN myocytes (100 nM dose) in basal conditions (data not shown).

Supplemental Fig. 1C demonstrates that the expression of Npr1 and Npr2 (corresponding to NPR-A and NPR-B proteins) is not altered in NPR-C$^{-/-}$ right atrial/SAN tissue indicating that the expression of the GC-linked NPRs is not remodeled in mice lacking functional NPR-C receptors. This is consistent with our electrophysiological data demonstrating that the effects of BNP and CNP in NPR-C$^{-/-}$ myocytes are very similar to wildtypes.

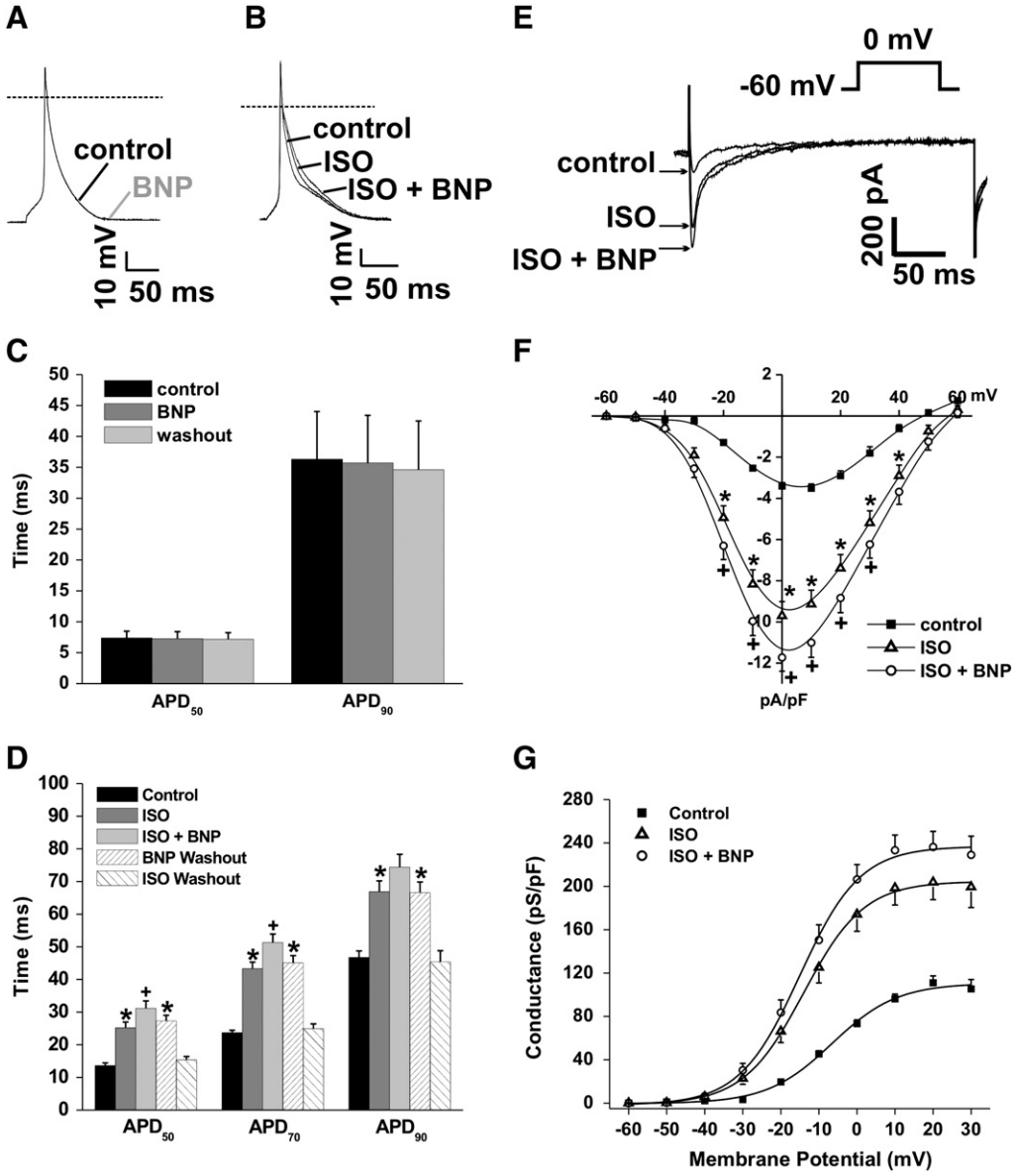

Fig. 5. Effects of BNP on right atrial myocyte action potentials and L-type Ca^{2+} current. The effects of BNP (100 nM) were studied in baseline conditions and in the presence of a submaximal dose of the β-adrenergic receptor agonist isoproterenol (ISO; 10 nM). Representative stimulated atrial myocyte APs illustrating the effects of BNP in baseline conditions (A) and in the presence of ISO (B). Dotted lines are at 0 mV. (C) Summary of the effects of BNP on right atrial AP duration in baseline conditions ($n=15$ myocytes). (D) Summary of the effects of BNP on right atrial AP duration in cells prestimulated with ISO ($n=12$ myocytes). (E) Representative right atrial $I_{Ca,L}$ recordings in control conditions, in the presence of ISO and following application of ISO + BNP. The voltage clamp protocol used (inset) allows measurement of $Ca_V1.2$ and $Ca_V1.3$ dependent $I_{Ca,L}$. (F) Summary right atrial myocyte $I_{Ca,L}$ I–V relationships in control conditions, in the presence of ISO and following application of BNP in the presence of ISO ($n=15$ right atrial myocytes). (G) Summary $I_{Ca,L}$ conductance density plots demonstrating the effects of ISO and BNP on $I_{Ca,L}$ activation kinetics. See Section 3.4 for details. $^*P<0.05$ vs. control, $^+P<0.05$ vs. ISO by one-way ANOVA with a Student–Newman–Keuls posthoc test.

3.7. Effects of BNP in the presence of the NPR-A antagonist A71915

We next focused on the possibility that the GC-linked NPRs are responsible for the NP effects described above by examining the effects of BNP on SAN and atrial myocytes in the presence of the NPR-A antagonist A71915 (500 nM) [30,31]. As illustrated in Fig. 7A the effect of BNP on spontaneous AP frequency was completely antagonized by A71915 (which had no effect on AP firing itself). Summary data (Fig. 7B; Supplemental Table 2) illustrate that spontaneous AP frequency was 150 ± 9.8 APs/min in control conditions, 147 ± 8.5 APs/min in A71915 and 153 ± 7.2 APs/min in A71915 + BNP ($P=0.97$). DD slope and all other AP parameters, were unaffected ($P=0.98$) by A71915 or BNP (Fig. 7C, Supplemental Table 2). Figs. 7D–G illustrate that, consistent with our AP measurements, A71915 completely blocked the ability of BNP to increase $I_{Ca,L}$ and I_f in SAN myocytes. Supplemental Fig. 5 illustrates that A71915 also completely antagonized the ability of BNP to increase $I_{Ca,L}$ in right atrial myocytes in the presence of ISO (10 nM). These data demonstrate that the stimulatory effects of BNP on SAN myocytes (basal conditions) and right atrial myocytes (submaximal doses of ISO) are NPR-A dependent.

3.8. Effects of BNP and CNP in the presence of the phosphodiesterase 3 inhibitor milrinone

NPR-A (which binds BNP) and NPR-B (which binds CNP) both activate GCs that increase intracellular cGMP [2,3]. cGMP modulates the activity of several signaling molecules that could mediate the effects of BNP and CNP on ion channels in the SAN and atria. For example, cGMP activates PKG and PDE2 and inhibits PDE3 [2,4]. PKG has been

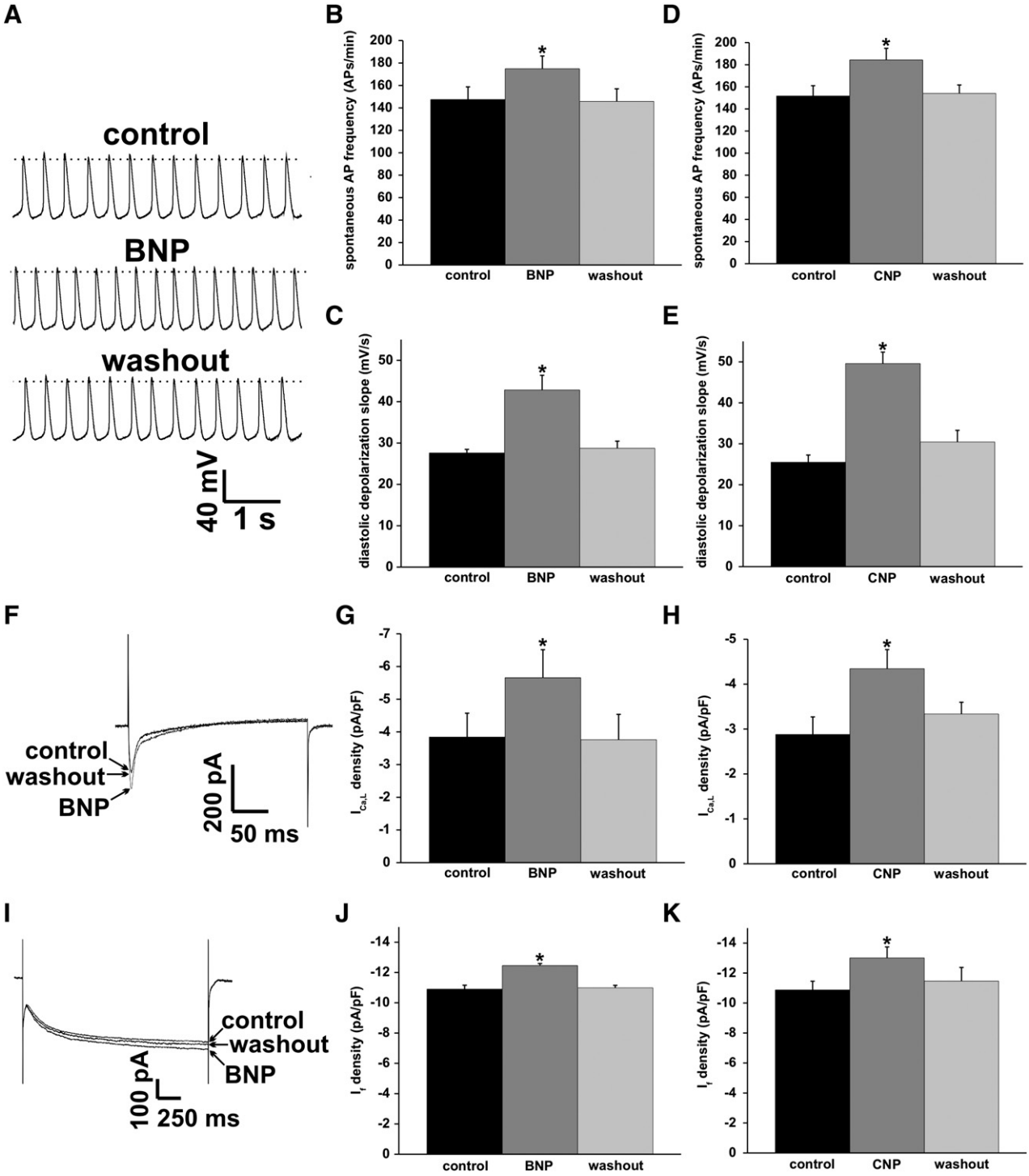

Fig. 6. Effects of BNP and CNP on isolated sinoatrial node myocytes isolated from mutant mice lacking functional NPR-C receptors (NPR-$C^{-/-}$). (A) Representative spontaneous AP recordings (5 s duration) in control conditions, following application of BNP (100 nM) and after wash off of BNP. Summary bar graphs illustrate the effects of BNP and CNP (100 nM) on spontaneous AP frequency (B and D) and diastolic depolarization slope (C and E) in NPR-$C^{-/-}$ mice ($n=7$ SAN myocytes for each peptide). (F) Representative $I_{Ca,L}$ recordings at −10 mV in SAN myocytes from NPR-$C^{-/-}$ mice in control conditions, in the presence of BNP, and after BNP washout. (G and H) Summary of the effects of BNP and CNP on $I_{Ca,L}$ density at −10 mV in NPR-$C^{-/-}$ SAN myocytes ($n=5$ SAN myocytes for each peptide). (I) Representative I_f recordings at −120 mV in SAN myocytes from NPR-$C^{-/-}$ mice in control conditions, in the presence of BNP, and after BNP washout. (J and K) Summary of the effects of BNP and CNP on I_f density at −120 mV in NPR-$C^{-/-}$ SAN myocytes ($n=5$ SAN myocytes for each peptide). *$P<0.05$ vs. control by one-way ANOVA with a Tukey posthoc test.

shown to decrease $I_{Ca,L}$ in cardiomyocytes [32–34] and activation of PDE2 also reduces $I_{Ca,L}$ by increasing the hydrolysis of cAMP [35,36]. Inhibition of PDE3 by cGMP, on the other hand, reduces the hydrolysis of cAMP, which leads to an increase in $I_{Ca,L}$ [37–39]. Since our data show that BNP and CNP increase $I_{Ca,L}$ in an NPR-A/NPR-B-dependent fashion we hypothesized that these effects involve PDE3. This was evaluated by applying BNP or CNP in the presence of the PDE3 inhibitor milrinone (Mil, 10 μM) [40,41].

As illustrated in Fig. 8A the ability of BNP (100 nM) to increase spontaneous AP frequency in SAN myocytes was completely absent in cells that were pretreated with Mil (10 μM). On average, Mil increased ($P<0.05$) AP frequency from 138 ± 3.5 to 180 ± 13.9 APs/min

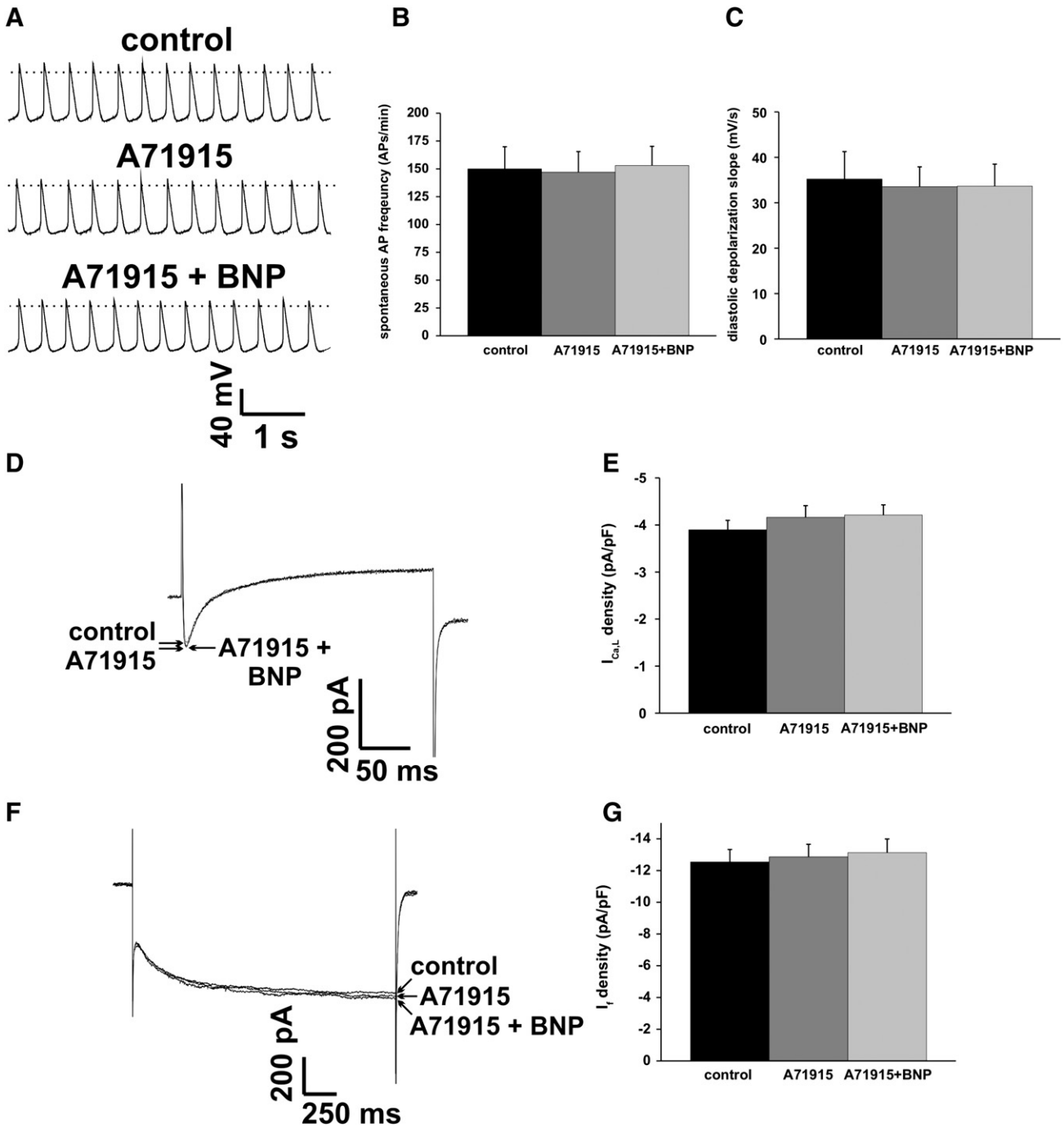

Fig. 7. Effects of BNP on sinoatrial node myocytes in the presence of the NPR-A antagonist A71915. (A) Representative spontaneous AP recordings in control conditions, in the presence of A71915 (500 nM) and following application of BNP (100 nM) in the presence of A71915. (B and C) Summary data showing the lack of effect of BNP on spontaneous AP frequency and diastolic depolarization slope after NPR-A blockade with A71915 ($n=5$ SAN myocytes). (D and E) Representative recordings and summary data ($n=5$ SAN myocytes) illustrating the lack of effect of BNP on $I_{Ca,L}$ at −10 mV in the presence of A71915. (F and G) Representative recordings and summary data ($n=5$ SAN myocytes) illustrating the lack of effect of BNP on I_f at −120 mV in the presence of A71915. Data were analyzed by one-way ANOVA with a Tukey posthoc test.

(Fig. 8B) and DD slope from 27.7 ± 2.7 to 48 ± 6.5 mV/s (Fig. 8C). Application of BNP in the presence of Mil had no further effect ($P=0.99$) on AP frequency (182 ± 13 APs/min) or DD slope (45.9 ± 6.7). Very similar effects were observed when CNP was applied in the presence of Mil (Figs. 8D and E).

Consistent with these AP data BNP and CNP had no effect on $I_{Ca,L}$ or I_f in SAN myocytes treated with Mil (Fig. 8). $I_{Ca,L}$ and I_f density were increased ($P<0.05$) by Mil; however, application of BNP($P=0.89$) or CNP ($P=0.75$) in the presence of Mil caused no further change in these currents. The effects of Mil (10 μM) and BNP (100 nM) were also evaluated in right atrial myocytes in the presence of ISO (10 nM; Supplemental Fig. 6). These data demonstrate that ISO increased ($P<0.05$) atrial $I_{Ca,L}$ from −2.1 ± 0.1 to −5.8 ± 0.7 pA/pF and application of Mil in the presence of ISO further increased ($P<0.05$) $I_{Ca,L}$ to −7.3 ± 0.6 pA/pF; however, BNP applied in the presence of Mil and ISO had no effect ($P=0.60$) on atrial $I_{Ca,L}$ (−7.4 ± 0.6 pA/pF).

Together these data suggest that NPs affect SAN and atrial electrophysiological properties in these conditions in a PDE3-dependent fashion. To further test this hypothesis two additional experiments were performed in isolated right atrial myocytes. First the effects of Mil (10 μM) on atrial $I_{Ca,L}$ were measured in basal

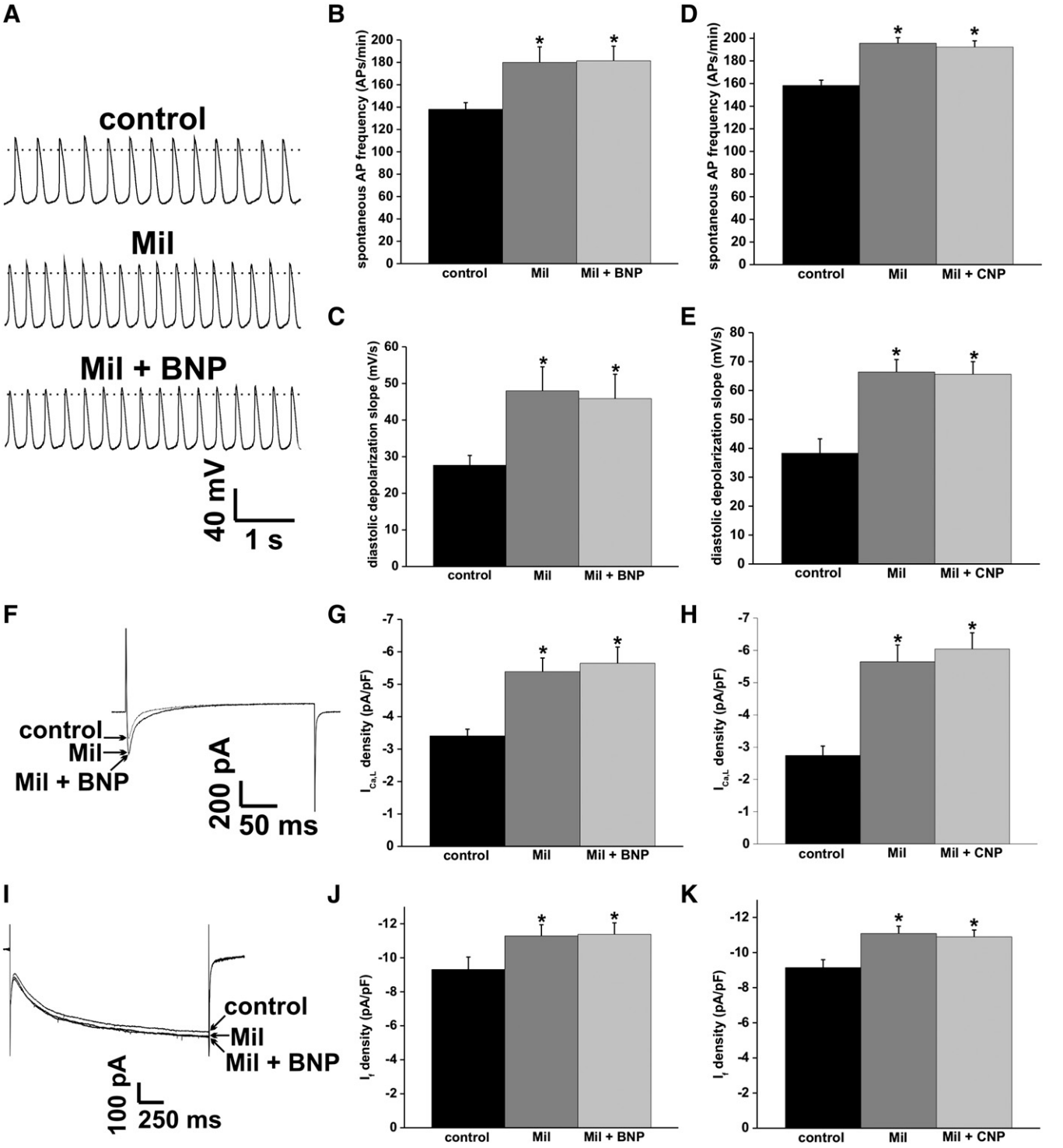

Fig. 8. Effects of BNP and CNP on sinoatrial node myocytes in the presence of the phosphodiesterase 3 inhibitor milrinone. (A) Representative spontaneous AP recordings (5 s duration) in control conditions, in the presence of Mil (10 μM) and after application of BNP (100 nM) in the presence of Mil. Summary bar graphs illustrating the effects of BNP and CNP (100 nM) on spontaneous AP frequency (B and D) and diastolic depolarization slope (C and E) following inhibition of PDE3 with Mil ($n = 5$ SAN myocytes for BNP and 7 SAN myocytes for CNP). (F) Representative $I_{Ca,L}$ recordings at −10 mV in SAN myocytes in control conditions, in the presence of Mil, and after application of BNP in the presence of Mil. (G and H) Summary of the effects of BNP and CNP on SAN myocyte $I_{Ca,L}$ density at −10 mV following application of Mil ($n = 5$ SAN myocytes for each peptide). (I) Representative I_f recordings at −120 mV in SAN myocytes in control conditions, in the presence of Mil, and after application of BNP in the presence of Mil. (J and K) Summary of the effects of BNP and CNP on I_f density at −120 mV in the presence of Mil ($n = 5$ SAN myocytes for each peptide). *$P<0.05$ vs. control by one-way ANOVA with a Tukey posthoc test. BNP and CNP had no effect on SAN AP firing, $I_{Ca,L}$ or I_f in the presence of Mil.

conditions (Supplemental Fig. 7). Unlike SAN myocytes (Fig. 8) Mil had no effect ($P = 0.43$) on basal atrial $I_{Ca,L}$ indicating that atrial myocytes do not have constitutive PDE3 activity. This may explain the lack of effect of BNP on atrial myocytes in basal conditions (see Discussion). Second, we confirmed that the absence of a BNP effect in the presence of ISO and Mil was not due to atrial $I_{Ca,L}$ having reached a state of maximum conductance before application of BNP by showing that atrial $I_{Ca,L}$ in the presence of ISO and Mil can be further increased ($P<0.05$) by applying the broad spectrum PDE inhibitor IBMX (100 μM; Supplemental Fig. 8).

4. Discussion

The present investigation shows that BNP and CNP can potently increase HR and electrical conduction in basal conditions. These effects are associated with increases in the frequency of spontaneous AP firing in isolated SAN myocytes due, at least in part, to increases in $I_{Ca,L}$ and I_f (two currents known to contribute prominently to the DD [18]). BNP and CNP were used as agonists so that the roles of all three NPRs could be assessed. Our data show that in basal conditions BNP and CNP primarily elicit their effects via the GC-linked NPR-A and NPR-B receptors because the effects of BNP were completely antagonized by the NPR-A antagonist A71915 (which prevents ANP and BNP from increasing cGMP [30,42]). Furthermore, BNP and CNP both increased AP frequency in SAN myocytes from NPR-$C^{-/-}$ mice as effectively as in wildtype myocytes. Although we have not directly measured changes in cGMP, it is well established that activation of NPR-A and NPR-B results in increased cGMP levels in the heart [2,43], thus it is suggested that the functional electrophysiological changes we have observed coincide with changes in cGMP downstream of NPR-A and NPR-B activation.

Although NPRs are known to be expressed in the heart [44,45], our study provides the first quantitative assessment of NPR expression in the SAN in comparison to the working right atrial myocardium. Despite some differences in NPR mRNA expression (Npr1 was more highly expressed than Npr2 in SAN myocytes) our functional data in isolated hearts and isolated SAN myocytes show that BNP and CNP elicited very comparable effects suggesting that there is sufficient NPR-A and NPR-B protein expression in SAN myocytes to produce similar amounts of GC activation. Furthermore, although the expression of Npr1 and Npr2 was relatively low in atrial myocytes, our immunocytochemical data confirm that NPR-A and NPR-B proteins are present in atrial myocytes and our functional data clearly suggest that there is sufficient receptor expression to enable NPs to elicit electrophysiological effects in the heart.

The effects of BNP were also measured in right atrial myocytes based on the ability of BNP (and CNP) to speed conduction through the atria and AV node in basal conditions. Interestingly, BNP had no effect on atrial APs in basal conditions; however, in the presence of a submaximal (10 nM) concentration of ISO BNP prolonged atrial AP duration and increased $I_{Ca,L}$ by a similar mechanism to the SAN. These data suggest that the increase in conduction across the atria in basal conditions may occur due to the increase in HR and SAN activity, but that in the presence of ISO NPs may also affect atrial conduction due to direct effects on $I_{Ca,L}$ that alter atrial AP duration.

NP signaling is complex because cGMP can modify the activity of several signaling proteins including PKG, PDE2 and PDE3 [2,3]. Our efforts to identify the molecular mechanism by which BNP and CNP increase HR and electrical conduction suggest that PDE3, which is well known to be inhibited by cGMP [37,38,46] is a critical target of NPs. This conclusion is based on several observations including: (1) the effects of BNP and CNP on isolated SAN myocytes (basal conditions) and atrial myocytes (in submaximal doses of ISO) are completely lost following inhibition of PDE3 with Mil. (2) Mil itself has very similar stimulatory effects to BNP and CNP in SAN myocytes (basal conditions) and atrial myocytes (in submaximal doses of ISO). (3) PDE3 inhibition with Mil has no effect on atrial $I_{Ca,L}$ in basal conditions indicating that atrial myocytes do not have constitutive PDE3 activity. This means that in these conditions there is no PDE3 activity for BNP to target, which may explain why BNP had no effect on atrial myocytes in basal conditions. In contrast, SAN myocytes do possess constitutive PDE3 activity (as indicated by the ability of Mil to increase AP firing and ionic currents in basal conditions), which is consistent with prior studies showing constitutive PDE3 activity in rabbit SAN [47]. This difference in PDE3 activity between SAN and atrial myocytes results in a differential sensitivity of ion channels in these two regions of the myocardium to NPs in basal conditions. (4) the lack of effect of BNP on $I_{Ca,L}$ in atrial myocytes is not due to the channel reaching a maximum conductance state before application of BNP because the nonspecific PDE inhibitor IBMX was able to increase $I_{Ca,L}$ in atrial myocytes that had been treated with ISO and Mil. This demonstrates that BNP cannot increase $I_{Ca,L}$ in the presence of Mil due to the specific blockade of PDE3.

Based on these data we propose that BNP and CNP increase HR and electrical conduction by activating their GC-linked NPR-A and NPR-B receptors, increasing intracellular cGMP and inhibiting PDE3. Inhibition of PDE3 would be expected to result in an increase in intracellular cAMP [37,38]. Consistent with this hypothesis several studies have shown that NPs can inhibit PDE3 activity and alter cAMP signaling in the cardiovascular and other systems [14,43,48,49]. $I_{Ca,L}$ and I_f are modulated by cAMP [18] via PKA phosphorylation ($I_{Ca,L}$) or by direct cyclic nucleotide binding to HCN channels (although HCN channel activity may also be modulated by PKA [50]). Interestingly, our data show that NPs increase I_f density even at membrane potentials as negative as −160 mV. Since prior studies in rabbit SAN demonstrate that cAMP affects I_f by shifting the position of the activation curve without increasing maximum conductance [51] it is possible that the voltages at which cAMP no longer increases I_f in mouse SAN are more negative than in the rabbit. Indeed, we have previously observed increases in I_f at −160 mV upon application of ISO in mouse SAN myocytes [21]. Alternatively, given the complexity of NP signaling, it is possible that BNP and CNP have additional cAMP independent effects on HCN channels that further increase I_f. Additional experiments will be necessary to evaluate these possibilities.

There are several other ion channels and Ca^{2+} handling mechanisms that contribute to HR regulation in the SAN, which are cAMP sensitive. For example, the SR Ca^{2+} release/I_{NCX} mechanism that is active during the DD is modulated by PKA [17] and repolarization of the AP in SAN myocytes is at least partially dependent on a delayed rectifier K^+ current (I_{Kr}) that is sensitive to cAMP [52]. It is possible that these also contribute to the effects of NPs on HR and electrical conduction.

Activation of NPR-A/B increases cGMP that can activate PKG and PDE2 in addition to inhibiting PDE3 [2] and studies have shown that PDE2 and PKG are involved in mediating or regulating NP effects in ventricular myocytes [53,54]. Which cGMP sensitive target dominates a physiological response may depend on a number of factors including the basal and stimulated levels of GC and adenylyl cyclase and the abundance and subcellular localization of the relevant signaling molecules, which can result in compartmentation of cGMP signaling [38,53]. NPs can also activate NPR-C, which is coupled to the activation of G_i proteins [5,6]. Although the present study clearly demonstrates NPR-C is not active in basal conditions we previously demonstrated that CNP can decrease HR by inhibiting $I_{Ca,L}$ in SAN myocytes [10,11] following activation of NPR-C in the presence of a maximum dose (1 μM) of ISO. Future studies will be needed to determine the conditions in which PKG and PDE2 are modulated by NPs in the SAN and atrial myocardium and how the GC-linked NPR-A and NPR-B receptors and NPR-C function together to determine overall physiological responses.

In summary, the present study provides novel insight into the mechanisms by which NPs regulate heart rate and electrical conduction, which include direct effects within the specialized pacemaker myocytes of the SAN as well as the working atrial myocardium. NPs are powerful regulators of cardiac performance with great promise for therapeutic use in cardiac disease states. Our findings advance our understanding of how NPs directly regulate HR, which is a critical determinant of cardiac output, and show that BNP and CNP primarily signal through NPR-A and NPR-B, but not NPR-C in basal conditions. These effects involve crosstalk between cGMP and cAMP via PDEs which is emerging as an important regulatory mechanism in the heart in normal and pathophysiological conditions [55].

Funding

This work was supported by operating grants from the Canadian Institutes of Health Research (MOP 93718), the Heart and Stroke Foundation of Nova Scotia and the Dalhousie Medical Research Foundation to RAR who is a CIHR New Investigator. JS was supported by a studentship from the Nova Scotia Health Research Foundation.

Disclosure statement

None.

Appendix A. Supplementary data

Supplementary data to this article can be found online at doi:10.1016/j.yjmcc.2012.01.018.

References

[1] Levin ER, Gardner DG, Samson WK. Natriuretic peptides. N Engl J Med 1998;339:321–8.
[2] Potter LR, Abbey-Hosch S, Dickey DM. Natriuretic peptides, their receptors, and cyclic guanosine monophosphate-dependent signaling functions. Endocr Rev 2006;27:47–72.
[3] Lucas KA, Pitari GM, Kazerounian S, Ruiz-Stewart I, Park J, Schulz S, et al. Guanylyl cyclases and signaling by cyclic GMP. Pharmacol Rev 2000;52:375–414.
[4] Kuhn M. Molecular physiology of natriuretic peptide signalling. Basic Res Cardiol 2004;99:76–82.
[5] Pagano M, Anand-Srivastava MB. Cytoplasmic domain of natriuretic peptide receptor C constitutes Gi activator sequences that inhibit adenylyl cyclase activity. J Biol Chem 2001;276:22064–70.
[6] Zhou H, Murthy KS. Identification of the G protein-activating sequence of the single-transmembrane natriuretic peptide receptor C (NPR-C). Am J Physiol 2003;284:C1255–61.
[7] Cataliotti A, Chen HH, Redfield MM, Burnett Jr JC. Natriuretic peptides as regulators of myocardial structure and function: pathophysiologic and therapeutic implications. Heart Fail Clin 2006;2:269–76.
[8] Lee CY, Burnett Jr JC. Natriuretic peptides and therapeutic applications. Heart Fail Rev 2007;12:131–42.
[9] Rose RA. CD-NP, a chimeric natriuretic peptide for the treatment of heart failure. Curr Opin Investig Drugs 2010;11:349–56.
[10] Rose RA, Lomax AE, Kondo CS, Anand-Srivastava MB, Giles WR. Effects of C-type natriuretic peptide on ionic currents in mouse sinoatrial node: a role for the NPR-C receptor. Am J Physiol Heart Circ Physiol 2004;286:H1970–7.
[11] Rose RA, Giles WR. Natriuretic peptide C receptor signalling in the heart and vasculature. J Physiol 2008;586:353–66.
[12] Beaulieu P, Cardinal R, De LA, Lambert C. Direct chronotropic effects of atrial and C-type natriuretic peptides in anaesthetized dogs. Br J Pharmacol 1996;118:1790–6.
[13] Beaulieu P, Cardinal R, Page P, Francoeur F, Tremblay J, Lambert C. Positive chronotropic and inotropic effects of C-type natriuretic peptide in dogs. Am J Physiol 1997;273:H1933–40.
[14] Herring N, Zaman JA, Paterson DJ. Natriuretic peptides like NO facilitate cardiac vagal neurotransmission and bradycardia via a cGMP pathway. Am J Physiol 2001;281:H2318–27.
[15] DiFrancesco D. Pacemaker mechanisms in cardiac tissue. Annu Rev Physiol 1993;55:455–72.
[16] Irisawa H, Brown HF, Giles W. Cardiac pacemaking in the sinoatrial node. Physiol Rev 1993;73:197–227.
[17] Lakatta EG, Maltsev VA, Vinogradova TM. A coupled SYSTEM of intracellular Ca^{2+} clocks and surface membrane voltage clocks controls the timekeeping mechanism of the heart's pacemaker. Circ Res 2010;106:659–73.
[18] Mangoni ME, Nargeot J. Genesis and regulation of the heart automaticity. Physiol Rev 2008;88:919–82.
[19] Jaubert J, Jaubert F, Martin N, Washburn LL, Lee BK, Eicher EM, et al. Three new allelic mouse mutations that cause skeletal overgrowth involve the natriuretic peptide receptor C gene (Npr3). Proc Natl Acad Sci U S A 1999;96:10278–83.
[20] Cifelli C, Rose RA, Zhang H, Voigtlaender-Bolz J, Bolz SS, Backx PH, et al. RGS4 regulates parasympathetic signaling and heart rate control in the sinoatrial node. Circ Res 2008;103:527–35.
[21] Rose RA, Kabir MG, Backx PH. Altered heart rate and sinoatrial node function in mice lacking the cAMP regulator phosphoinositide 3-kinase-gamma. Circ Res 2007;101:1274–82.
[22] Marionneau C, Couette B, Liu J, Li H, Mangoni ME, Nargeot J, et al. Specific pattern of ionic channel gene expression associated with pacemaker activity in the mouse heart. J Physiol 2005;562:223–34.
[23] Liu J, Dobrzynski H, Yanni J, Boyett MR, Lei M. Organisation of the mouse sinoatrial node: structure and expression of HCN channels. Cardiovasc Res 2007;73:729–38.
[24] Mangoni ME, Couette B, Bourinet E, Platzer J, Reimer D, Striessnig J, et al. Functional role of L-type Cav1.3 Ca2+ channels in cardiac pacemaker activity. Proc Natl Acad Sci U S A 2003;100:5543–8.
[25] Zhang Z, Xu Y, Song H, Rodriguez J, Tuteja D, Namkung Y, et al. Functional roles of $Ca_v1.3$ ($alpha_{1D}$) calcium channel in sinoatrial nodes: insight gained using gene-targeted null mutant mice. Circ Res 2002;90:981–7.
[26] Rose RA, Sellan M, Simpson JA, Izaddoustdar F, Cifelli C, Panama BK, et al. Iron overload decreases CaV1.3-dependent L-type Ca^{2+} currents leading to bradycardia, altered electrical conduction, and atrial fibrillation. Circ Arrhythm Electrophysiol 2011;4:733–42.
[27] Zhang Z, He Y, Tuteja D, Xu D, Timofeyev V, Zhang Q, et al. Functional roles of Cav1.3(alpha1D) calcium channels in atria: insights gained from gene-targeted null mutant mice. Circulation 2005;112:1936–44.
[28] Rose RA, Lomax AE, Giles WR. Inhibition of L-type Ca^{2+} current by C-type natriuretic peptide in bullfrog atrial myocytes: an NPR-C-mediated effect. Am J Physiol 2003;285:H2454–62.
[29] Anand-Srivastava MB, Sairam MR, Cantin M. Ring-deleted analogs of atrial natriuretic factor inhibit adenylate cyclase/cAMP system. Possible coupling of clearance atrial natriuretic factor receptors to adenylate cyclase/cAMP signal transduction system. J Biol Chem 1990;265:8566–72.
[30] Delporte C, Winand J, Poloczek P, Von Geldern T, Christophe J. Discovery of a potent atrial natriuretic peptide antagonist for ANPA receptors in the human neuroblastoma NB-OK-1 cell line. Eur J Pharmacol 1992;224:183–8.
[31] Trachte GJ. Atrial natriuretic factor alters neurotransmission independently of guanylate cyclase-coupled receptors in the rabbit vas deferens. J Pharmacol Exp Ther 1993;264:1227–33.
[32] Lohmann SM, Fischmeister R, Walter U. Signal transduction by cGMP in heart. Basic Res Cardiol 1991;86:503–14.
[33] Mery PF, Lohmann SM, Walter U, Fischmeister R. Ca^{2+} current is regulated by cyclic GMP-dependent protein kinase in mammalian cardiac myocytes. Proc Natl Acad Sci U S A 1991;88:1197–201.
[34] Tohse N, Nakaya H, Takeda Y, Kanno M. Cyclic GMP-mediated inhibition of L-type Ca^{2+} channel activity by human natriuretic peptide in rabbit heart cells. Br J Pharmacol 1995;114:1076–82.
[35] Mery PF, Pavoine C, Pecker F, Fischmeister R. Erythro-9-(2-hydroxy-3-nonyl)adenine inhibits cyclic GMP-stimulated phosphodiesterase in isolated cardiac myocytes. Mol Pharmacol 1995;48:121–30.
[36] Rivet-Bastide M, Vandecasteele G, Hatem S, Verde I, Benardeau A, Mercadier JJ, et al. cGMP-stimulated cyclic nucleotide phosphodiesterase regulates the basal calcium current in human atrial myocytes. J Clin Invest 1997;99:2710–8.
[37] Bender AT, Beavo JA. Cyclic nucleotide phosphodiesterases: molecular regulation to clinical use. Pharmacol Rev 2006;58:488–520.
[38] Maurice DH, Palmer D, Tilley DG, Dunkerley HA, Netherton SJ, Raymond DR, et al. Cyclic nucleotide phosphodiesterase activity, expression, and targeting in cells of the cardiovascular system. Mol Pharmacol 2003;64:533–46.
[39] Vandecasteele G, Verde I, Rucker-Martin C, Donzeau-Gouge P, Fischmeister R. Cyclic GMP regulation of the L-type Ca^{2+} channel current in human atrial myocytes. J Physiol 2001;533:329–40.
[40] Kerfant BG, Zhao D, Lorenzen-Schmidt I, Wilson LS, Cai S, Chen SR, et al. PI3K-gamma is required for PDE4, not PDE3, activity in subcellular microdomains containing the sarcoplasmic reticular calcium ATPase in cardiomyocytes. Circ Res 2007;101:400–8.
[41] Verde I, Vandecasteele G, Lezoualc'h F, Fischmeister R. Characterization of the cyclic nucleotide phosphodiesterase subtypes involved in the regulation of the L-type Ca^{2+} current in rat ventricular myocytes. Br J Pharmacol 1999;127:65–74.
[42] Kumar R, Cartledge WA, Lincoln TM, Pandey KN. Expression of guanylyl cyclase-A/atrial natriuretic peptide receptor blocks the activation of protein kinase C in vascular smooth muscle cells. Role of cGMP and cGMP-dependent protein kinase. Hypertension 1997;29:414–21.
[43] Qvigstad E, Moltzau LR, Aronsen JM, Nguyen CH, Hougen K, Sjaastad I, et al. Natriuretic peptides increase beta1-adrenoceptor signalling in failing hearts through phosphodiesterase 3 inhibition. Cardiovasc Res 2010;85:763–72.
[44] Del RS, Cabiati M, Lionetti V, Giannessi D. NPR-B, the C-type natriuretic peptide specific receptor, is the predominant biological receptor in mouse and pig myocardial tissue. Minerva Endocrinol 2010;35:37–46.
[45] Nunez DJ, Dickson MC, Brown MJ. Natriuretic peptide receptor mRNAs in the rat and human heart. J Clin Invest 1992;90:1966–71.
[46] Omori K, Kotera J. Overview of PDEs and their regulation. Circ Res 2007;100:309–27.
[47] Vinogradova TM, Sirenko S, Lyashkov AE, Younes A, Li Y, Zhu W, et al. Constitutive phosphodiesterase activity restricts spontaneous beating rate of cardiac pacemaker cells by suppressing local Ca^{2+} releases. Circ Res 2008;102:761–9.
[48] Wen JF, Quan HX, Zhou GH, Cho KW. Altered role of C-type natriuretic peptide-activated pGC-cGMP-PDE3-cAMP signaling in hyperthyroid beating rabbit atria. Regul Pept 2007;142:123–30.
[49] Wen JF, Cui X, Jin JY, Kim SM, Kim SZ, Kim SH, et al. High and low gain switches for regulation of cAMP efflux concentration: distinct roles for particulate GC- and soluble GC-cGMP-PDE3 signaling in rabbit atria. Circ Res 2004;94:936–43.
[50] Liao Z, Lockhead D, Larson ED, Proenza C. Phosphorylation and modulation of hyperpolarization-activated HCN4 channels by protein kinase A in the mouse sinoatrial node. J Gen Physiol 2010;136:247–58.
[51] DiFrancesco D, Mangoni M. Modulation of single hyperpolarization-activated channels (i_f) by cAMP in the rabbit sino-atrial node. J Physiol 1994;474:473–82.

[52] Clark RB, Mangoni ME, Lueger A, Couette B, Nargeot J, Giles WR. A rapidly activating delayed rectifier K^+ current regulates pacemaker activity in adult mouse sinoatrial node cells. Am J Physiol 2004;286:H1757–66.
[53] Castro LR, Verde I, Cooper DM, Fischmeister R. Cyclic guanosine monophosphate compartmentation in rat cardiac myocytes. Circulation 2006;113:2221–8.
[54] Castro LR, Schittl J, Fischmeister R. Feedback control through cGMP-dependent protein kinase contributes to differential regulation and compartmentation of cGMP in rat cardiac myocytes. Circ Res 2010;107:1232–40.
[55] Zaccolo M, Movsesian MA. cAMP and cGMP signaling cross-talk: role of phosphodiesterases and implications for cardiac pathophysiology. Circ Res 2007;100:1569–78.

The natriuretic peptides BNP and CNP increase heart rate and electrical conduction by stimulating ionic currents in the sinoatrial node and atrial myocardium following activation of guanylyl cyclase-linked natriuretic peptide receptors

Online Supplement

Supplemental Methods

Animals

This study utilized male wildtype C57Bl/6 mice (Charles River) and mutant mice lacking functional NPR-C receptors (NPR-$C^{-/-}$). The NPR-$C^{-/-}$ mice were obtained from The Jackson Laboratory (strain B6;C-*Npr3*^{lgj}/J) and backcrossed into the C57Bl/6 line for more than 6 generations. This mouse contains a 36 base pair deletion (position 195-232) that results in the production of a nonfunctional NPR-C protein truncated by 12 amino acids in the extracellular domain [1]. All mice used in experiments were between the ages of 10-14 weeks. NPR-$C^{-/-}$ mice were genotyped using ear punch biopsies. All experimental procedures were in accordance with the regulations of The Canadian Council on Animal Care and were approved by the Dalhousie University animal care committee.

Electrocardiography in isolated hearts

ECGs were recorded in isolated Langendorff-perfused hearts as described previously [2]. In brief, mice were administered a 0.2 ml intraperitoneal injection of heparin (1000 IU/ml) to prevent blood clotting. Following this, mice were anesthetized by isoflurane inhalation and then killed by cervical dislocation. The heart was excised into Tyrode's solution (35ºC) consisting of (in mmol/L) 140 NaCl, 5.4 KCl, 1.2 KH_2PO_4, 1.0 $MgCl_2$, 1.8 $CaCl_2$, 5.55 glucose, and 5 HEPES, with pH adjusted to 7.4 with NaOH and cannulated via the aorta for retrograde aortic perfusion.

Hearts were perfused with oxygenated Tyrode's solution at a flow rate of 2.5 ml/min and allowed to stabilize for at least 10 min.

ECGs were acquired using needle electrodes (Grass Technologies) a Gould ACQ-7700 amplifier and the Ponemah Physiology Platform software (Data Sciences International). Standard ECG waves and intervals, including R-R interval, P wave duration, P-R interval, and Q-T interval, were analyzed.

Isolation of mouse sinoatrial node and right atrial myocytes

The procedures for isolating single pacemaker myocytes from the sinoatrial node (SAN), as well as working right atrial myocytes from the mouse have been described previously [3-6] and were as follows. Mice were administered a 0.2 ml intraperitoneal injection of heparin (1000 IU/ml) to prevent blood clotting. Following this, mice were anesthetized by isoflurane inhalation and then killed by cervical dislocation. The heart was excised into Tyrode's solution (35ºC) consisting of (in mmol/L) 140 NaCl, 5.4 KCl, 1.2 KH_2PO_4, 1.0 $MgCl_2$, 1.8 $CaCl_2$, 5.55 glucose, and 5 HEPES, with pH adjusted to 7.4 with NaOH. The sinoatrial node (SAN) region of the heart was isolated by separating the atria from the ventricles, cutting open the superior and inferior venae cavae, and pinning the tissue so that the crista terminalis could be identified. The SAN area is located in the intercaval region adjacent to the crista terminalis. This SAN region was cut into strips, which were transferred and rinsed in a 'low Ca^{2+}, Mg^{2+} free' solution containing (in mmol/L) 140 NaCl, 5.4 KCl, 1.2 KH_2PO_4, 0.2 $CaCl_2$, 50 taurine, 18.5 glucose, 5 HEPES and 1 mg/ml bovine serum albumin (BSA), with pH adjusted to 6.9 with NaOH. SAN tissue strips were digested in 5 ml of 'low Ca^{2+}, Mg^{2+} free' solution containing collagenase (type II, Worthington Biochemical Corporation), elastase (Worthington Biochemical Corporation) and

protease (type XIV, Sigma Chemical Company) for 30 min. Then the tissue was transferred to 5 ml of modified KB solution containing (in mmol/L) 100 potassium glutamate, 10 potassium aspartate, 25 KCl, 10 KH_2PO_4, 2 $MgSO_4$, 20 taurine, 5 creatine, 0.5 EGTA, 20 glucose, 5 HEPES, and 0.1% BSA, with pH adjusted to 7.2 with KOH. The tissue was mechanically agitated using a wide-bore pipette. This procedure yielded individual SAN myocytes with cellular automaticity that was recovered after readapting the cells to a physiological concentration of Ca^{2+}. The identical enzymatic procedure was used on tissue dissected from the right atrial appendage to isolate working right atrial myocytes.

SAN myocytes were identified by their small spindle shape and ability to beat spontaneously in the recording chamber when superfused with normal Tyrode's solution. When patch-clamped, SAN myocytes always displayed spontaneous action potentials and the hyperpolarization-activated current, I_f. The capacitance of single SAN myocytes was 20 – 35 pF. In contrast, working cardiomyocytes from the right atrium were larger than SAN myocytes, had stable resting membrane potentials, only fired action potentials in response to depolarizing current injection, and had membrane capacitances in the range of 40 – 65 pF.

Solutions and electrophysiological protocols

Spontaneous action potentials (APs) and stimulated APs were recorded using the perforated patch-clamp technique [7] on single SAN and right atrial myocytes. The hyperpolarization-activated current (I_f) and L-type Ca^{2+} currents ($I_{Ca,L}$) were primarily recorded by voltage clamping single SAN or right atrial myocytes using the patch-clamp technique in the whole cell configuration [8] although I_f was sometimes recorded using the perforated patch-

clamp technique. APs and membrane currents were recorded at room temperature (22-23 ºC), which must be noted when comparing these data to the isolated heart ECG experiments.

For recording APs and I_f the recording chamber was superfused with a normal Tyrode's solution (22 – 23ºC) containing (in mmol/L) 140 NaCl, 5 KCl, 1 $MgCl_2$, 1 $CaCl_2$, 10 HEPES, and 5 glucose, with pH adjusted to 7.4 with NaOH. The pipette filling solution for I_f contained (in mmol/L) 135 KCl, 0.1 $CaCl_2$, 1 $MgCl_2$, 5 NaCl, 10 EGTA, 4 Mg-ATP, 6.6 Na-phosphocreatine, 0.3 Na-GTP and 10 HEPES, with pH adjusted to 7.2 with KOH. Amphotericin B (200 µg/ml) was added to this pipette solution to record APs or I_f with the perforated patch clamp technique. $BaCl_2$ (1×10^{-4} mol/L) was added to the superfusate when recording I_f, in order to eliminate any inward rectifier K^+ current that could be present at low levels in some SAN myocytes [4].

For recording $I_{Ca,L}$ SAN and atrial myocytes were superfused with a modified Tyrode's solution (22 – 23ºC) containing the following (in mmol/L) 140 NaCl, 5.4 TEA-Cl, 3 $CaCl_2$, 1 $MgCl_2$, 10 HEPES, and 5 glucose with pH adjusted to 7.4 with NaOH. The pipette solution for $I_{Ca,L}$ contained (in mmol/L) 135 CsCl, 0.1 $CaCl_2$, 1 $MgCl_2$, 5 NaCl, 10 EGTA, 4 Mg-ATP, 6.6 Na-phosphocreatine, 0.3 Na-GTP and 10 HEPES, with pH adjusted to 7.2 with CsOH. To block voltage gated Na^+ currents (I_{Na}) when recording $I_{Ca,L}$ cells were treated with lidocaine (0.3 mM) or, in some cases, all external Na^+ was replaced with Cs^+. This approach was used in order to record SAN and atrial $I_{Ca,L}$ from a holding potential of -60 mV due to the expression of $Ca_V1.2$ and $Ca_V1.3$ in these cells [9-11].

Micropipettes were pulled from borosilicate glass (with filament, 1.5 mm OD, 0.75 mm ID, Sutter Instrument Company) using a Flaming/Brown pipette puller (model p-87, Sutter Instrument Company). The resistance of these pipettes was 4 – 8 MΩ when filled with recording

solution. Micropipettes were positioned with a micromanipulator (Burleigh PCS-5000 system) mounted on the stage of an inverted microscope (Olympus IX71). Seal resistance was 2 – 15 GΩ. Rupturing the sarcolemma in the patch for voltage clamp experiments resulted in access resistances of 5 – 15 MΩ. Series resistance compensation averaged 80 – 85% using an Axopatch 200B amplifier (Molecular Devices). For perforated patch clamp experiments access resistance was monitored for the development of capacitative transients upon sealing to the cell membrane with Amphotericin B in the pipette. Typically, access resistance became less than 30 MΩ within 5 min of sealing onto the cell, which was sufficient for recording spontaneous APs in current clamp mode. Data were digitized using a Digidata 1440 and pCLAMP 10 software (Molecular Devices) and stored on computer for *post hoc* analysis.

Spontaneous AP parameters, including the maximum diastolic potential (MDP), the slope of the diastolic depolarization (DD slope), the maximum AP upstroke velocity (Vmax), the AP overshoot and the AP duration at 50% repolarization (APD_{50}) were analyzed as described previously [4,12]. The DD slope was measured by fitting a straight line to the initial linear portion (~two-thirds) of this AP component [12].

Activation kinetics for I_f were determined by normalizing tail currents at each voltage to the maximum current level at -160 mV and fitting the data to the Boltzmann function: $I/I_{max}=1/(1+\exp[(V_m-V_{1/2})/k])$ where V_m is the potential of the voltage clamp step, $V_{1/2}$ is the voltage at which 50% activation occurs and k is the slope factor. $I_{Ca,L}$ activation kinetics were determined by calculating chord conductance (G) with the equation $G=I/(V_m-E_{rev})$, where V_m represents the depolarizing voltages and E_{rev} is the reversal potential estimated from the current-voltage relation of $I_{Ca,L}$. Maximum conductance (G_{max}) and $V_{1/2}$ of activation for $I_{Ca,L}$ were determined using the following function: $G=\{(V_m-V_{rev})\}\{G_{max}\}\{-1/[(1+\exp((V_m-V_{1/2})/k))+1]\}$.

The voltage clamp protocols and examples of I_f and $I_{Ca,L}$ recordings used to generate I-V relationships and to perform activation analysis are illustrated in Supplemental Fig. 9. I_f I-V relationships were determined from the peak current density at the end of the 2 s voltage clamp steps. The resultant I-V relationships, including apparent reversal potential, are highly comparable to those we [5,6,13] and others [4,14,15] have measured in previous studies using similar protocols.

Quantitative PCR

Quantitative gene expression studies were performed using an approach similar to Marionneau et al. [16] in which SAN and right atrial tissue samples were separately dissected for mRNA analysis. In order to have sufficient RNA 5 SAN samples were pooled for each individual trial as described previously [16]. Tissue samples were flash frozen in liquid nitrogen following dissection.

Intron spanning primers were designed for Npr1, Npr2 and Npr3 (genes corresponding to NPR-A, NPR-B and NPR-C) as well as GAPDH (reference gene) and tested using Amplify 3 (software for simulating and testing polymerase chain reactions). Following synthesis (Sigma Genosys) primers were reconstituted to 100 µM in nuclease free water and stored at -20 C until experimental use. Primer sequences were as follows: Npr1: forward 5`-CGAAGCTTCCAAGGTGTGACAGG-3`; reverse 5`-GACACAGCCATCAGCTCCTGGG-3`; amplification product 152 base pairs. Npr2: forward 5`-GGGGACTTTCAGCCCGCAGC-3`; reverse 5`- GTGGAGTTTTATCACAGGATGGGTCG-3`; amplification product 150 base pairs. Npr3: forward 5`-CGAGCGAGTGGTGATCATGTGTG-3`; reverse 5`-CTCCACGAGCCATCTCCGTAGG-3`; amplification product 147 base pairs. GAPDH: forward

5`-GTGCCAGCCTCGTCCCG-3`; reverse 5`-CCATGTAGTTGAGGTCAATGAAGGG-3`; amplification product 151 base pairs.

RNA was extracted in PureZOL ™ RNA isolation reagent according to kit instructions (Aurum™ total RNA fatty and fibrous tissue kit, BioRad). SAN tissue was eluted in 30 µl of elution buffer (provided) and right atrial RNA was eluted in 40µl from the spin column. RNA concentrations were determined using a Qubit fluorometer (Invitrogen) and first strand synthesis reactions were performed using the iScript™ cDNA synthesis kit (BioRad) according to kit directives with 0.5ug RNA template for right atrial samples. SAN samples were not quantified as initial screening indicated that RNA template concentrations in these samples were limiting. Instead, all 30 µl of the RNA extract obtained from SA node samples were used in first strand synthesis. A260/280 readings were also performed to evaluate the purity of RNA extractions prior to first strand synthesis. Lack of genomic DNA contamination was verified by reverse transcription (RT)-PCR using a no RT control.

SYBER green RT-qPCR was used to assess gene expression in 5 distinct pools of tissue. Following RNA extraction cDNA was synthesized for right atrial tissue and SAN tissue samples. 20 µl SYBR reactions were performed with 1 µl cDNA template used in right atrial samples and 2 µl cDNA template in SAN samples. (Varying concentrations were used to obtain data that crossed threshold for both sample types at similar cycles). Reactions were carried out using a CFX96 Real-Time PCR Detection System (BioRad). Amplification conditions were as follows: 95^0C for 2 min to activate Taq polymerase, 35 cycles of denaturation at 95^0C for 30 sec, annealing using a gradient from 53-61^0C for 30 sec and extension at 72^0C or 1 min 30 sec. Melt curve analysis was performed from 65-95^0C every 0.5^0C increments.

Single amplicons with appropriate melting temperatures and sizes were detected. Data were expressed in the form 2^{-CT} x 100 *versus* GAPDH for all tissue samples. C_T values > 32 were eliminated due to lack of reproducibility [16]. Primers were used at a concentration of 10μM.

Immunocytochemistry

NPR protein expression in SAN and right atrial myocytes was assessed by immunocytochemistry using approaches similar to those described previously [17]. For the detection of NPR proteins, goat anti-NPR-A polyclonal antibody (US Biologicals) was used at 1:250, rabbit anti-NPR-B polyclonal antibody (US Biologicals) was used at 1:50 and rabbit anti-NPR-C polyclonal antibody (US Biologicals) was used at 1:250. For HCN4 detection, rabbit anti-HCN4 polyclonal antibody (Alomone Labs) was used at 1:50. Secondary antibodies used in this experiment were rabbit anti goat Alexa Fluor 488 conjugated polyclonal antibody (Invitrogen) and goat anti rabbit Alexa Fluor 488 conjugated polyclonal antibody (Invitrogen). Secondary antibodies were used at 1:250.

50 μl of freshly isolated SAN or right atrial myocyte cell suspension was placed onto 0.1% poly-L-lysine coated slides and allowed to settle for 30 min. Cells were gently rinsed with 0.01 M phosphate buffered saline (PBS), pH 7.4, fixed with 4 % paraformaldehyde for 8 min at 4^0C then rinsed once more with 1x PBS.

Cells were washed with 0.01 M PBS for 15 min followed by a 10 min wash in 0.01M PBS containing 0.1% Triton X-100 then another 10 min wash in 0.01 M PBS. Cells were blocked with 1:20 horse serum in 0.01 M PBS for 30 min at room temperature, followed by a 5 min rinse in 0.01 M PBS. Cells were then incubated with primary antibody diluted in 1% BSA in

PBS over night at 4^0C. Slides were rinsed again for 15 min with 0.01 M PBS then incubated with secondary antibody diluted in 0.01 M PBS for 1 h at room temperature in the dark. Slides were washed for 15 min in 0.01 M PBS then for 5 min in ddiH_2O before being mounted using Hard Set mounting media (Vector Labs). Images were captured using a Zeiss LSM 510 confocal microscope.

Pharmacological compounds

BNP, CNP, cANF and A71915 were obtained from Bachem, dissolved in water, and stored in small aliquots (-80°C) until added to Tyrode's solution for experimental use. Isoproterenol, milrinone and IBMX were obtained from Sigma Chemical Company. ISO was dissolved in water while the PDE inhibitors were dissolved in dimethyl sulfoxide (DMSO; final concentration 0.01%).

Supplemental Results

Supplemental Table 1. Effects of BNP and CNP on ECG parameters in isolated Langendorff-perfused hearts.

	Control	BNP (500 nM)	Washout	Control	CNP (500 nM)	Washout
HR	348±14	437±23*	346±15	379±27	469±15*	377±25
R-R Interval	177.4±6.0	147.6±4.6*	178±6.6	168.4±13.0	129.6±4.1*	169.8±14.3
P wave duration	9.8±0.7	8.3±1.3*	9.7±0.8	10.4±0.6	8.3±0.3*	10.4±0.7
P-R Interval	51.7±3.1	37.8±0.9*	53.5±2.6	39.2±2.6	28.2±1.1*	40.6±2.7
Q-T Interval	65.4±9.5	57.9±8.7*	65.8±9.5	54.2±3.8	44.8±2.5*	54.6±4.2

HR, heart rate. P-R interval was measured from the start of the P wave to the peak of the QRS complex. Q-T interval was measured from the start of the QRS complex to the end of the T wave. Data are means ± SEM; n = 4 hearts for 100 nM group, n = 4 hearts for 300 nM group and n = 5 hearts for 500 nM group. *P<0.05 vs. control by one way ANOVA with a Tukey posthoc test.

Supplemental Table 2. Effects of BNP on spontaneous action potential parameters in isolated SAN myocytes.

	WT mice		NPR-C$^{-/-}$ mice		WT mice			WT mice		
n	8		7		5			5		
group	Control	BNP	Control	BNP	Control	A71915	A71915 + BNP	Control	Mil	Mil + BNP
Beating rate (APs/min)	148 ± 4.5	183 ± 6.3*	147 ± 11.3	175 ± 11.4*	150 ± 9.8	147 ± 8.5	153 ± 7.2	138 ± 3.5	180 ± 13.9†	182 ± 13.0†
MDP (mV)	-66.3 ± 0.9	-66.3 ± 0.8	-61.4 ± 1.8	-62 ± 1.7	-67.5 ± 1.5	-68.8 ± 1.6	-68.2 ± 1.8	-67 ± 4.0	-67.3 ± 1.7	-67.6 ± 2.0
DD slope (mV/s)	31.0 ± 1.7	48.3 ± 1.3*	27.6 ± 0.9	42.8 ± 3.5*	35.2 ± 6.1	33.6 ± 4.4	33.8 ± 4.8	27.7 ± 2.7	48 ± 6.5†	45.9 ±6.7†
V_{max} (V/s)	21.2 ± 10.7	24.6 ± 12.9	13.3 ± 7.4	10.4 ± 3.8	13.6 ± 9.0	14.9 ± 14.1	15.2 ± 10.2	15.2 ± 3.2	18.3 ± 5.7	19.9 ± 3.4
OS (mV)	14.2 ± 2.4	14.5 ± 2.0	5.0 ± 0.7	5.8 ± 1.2	9.4 ± 1.5	10.6 ± 3.3	8.9 ± 5.3	3.9 ± 0.5	5.4 ± 0.5	4.6 ± 0.6
APD_{50} (ms)	48.3 ± 4.8	54.3 ± 4.1*	54.5 ± 2.8	60.1 ± 2.8*	60.5 ± 8.1	56.8 ± 8.2	57.9 ± 5.4	50 ± 0.4	56.8 ± 0.5†	58.7 ± 0.5†

WT, wildtype; NPR-C$^{-/-}$, NPR-C mutant mice; *n*, sample size; MDP, maximum diastolic potential; DD slope, diastolic depolarization slope; V_{max}, maximum AP upstroke velocity; OS, overshoot; APD_{50}, AP duration at 50% repolarization; Mil, milrinone. BNP was applied at 100 nM, A71915 (NPR-A antagonist) was applied at 500 nM, Mil (PDE3 inhibitor) was applied at 10 μM. Data are means ± SEM; *P<0.05 vs. control by paired Student's t-test; $^{\dagger}P$<0.05 vs. control by one way ANOVA with a Tukey posthoc test.

Supplemental Table 3. Effects of CNP on spontaneous action potential parameters in isolated SAN myocytes.

	WT mice		NPR-C$^{-/-}$ mice		WT mice		
n	8		8		7		
group	Control	CNP	Control	CNP	Control	Mil	Mil + CNP
Beating rate (APs/min)	141 ± 12.2	168 ± 13*	152 ± 9.3	184 ± 10.5*	158 ± 4.7	195 ± 4.8†	192 ± 5.1†
MDP (mV)	-65.3 ± 2.0	-65.5 ± 2.4	-64.3 ± 2.2	-64 ± 2.1	-67.7 ± 4.0	-67.7 ± 0.6	-67.3 ± 0.5
DD slope (mV/s)	25.8 ± 4.6	43.1 ± 7.2*	25.4 ± 1.8	49.6 ± 2.8*	38.3 ± 5	56.4 ± 4.3†	55.6 ± 4.4†
V_{max} (V/s)	13.3 ± 5.3	13.8 ± 5.9	26.2 ± 5.9	22 ± 4.6	13.4 ± 3.0	16.9 ± 3.2	14 ± 3.2
OS (mV)	4.9 ± 1.3	5.8 ± 2.1	10.6 ± 0.9	7.4 ± 1.5	8.2 ± 1.9	10.1 ± 1	9.9 ± 1.3
APD_{50} (ms)	40.6 ± 3.6	48.5 ± 4.4*	55 ± 6.4	61.1 ± 4.4*	51.3 ± 4.9	59 ± 4.9†	58.4 ± 5†

WT, wildtype; NPR-C$^{-/-}$, NPR-C mutant mice; *n*, sample size; MDP, maximum diastolic potential; DD slope, diastolic depolarization slope; V_{max}, maximum AP upstroke velocity; OS, overshoot; APD_{50}, AP duration at 50% repolarization; Mil, milrinone. CNP was applied at 100 nM, Mil (PDE3 inhibitor) was applied at 10 µM. Data are means ± SEM; *P<0.05 vs. control by paired Student's t-test; $^{\dagger}P$<0.05 vs. control by one way ANOVA with a Tukey posthoc test.

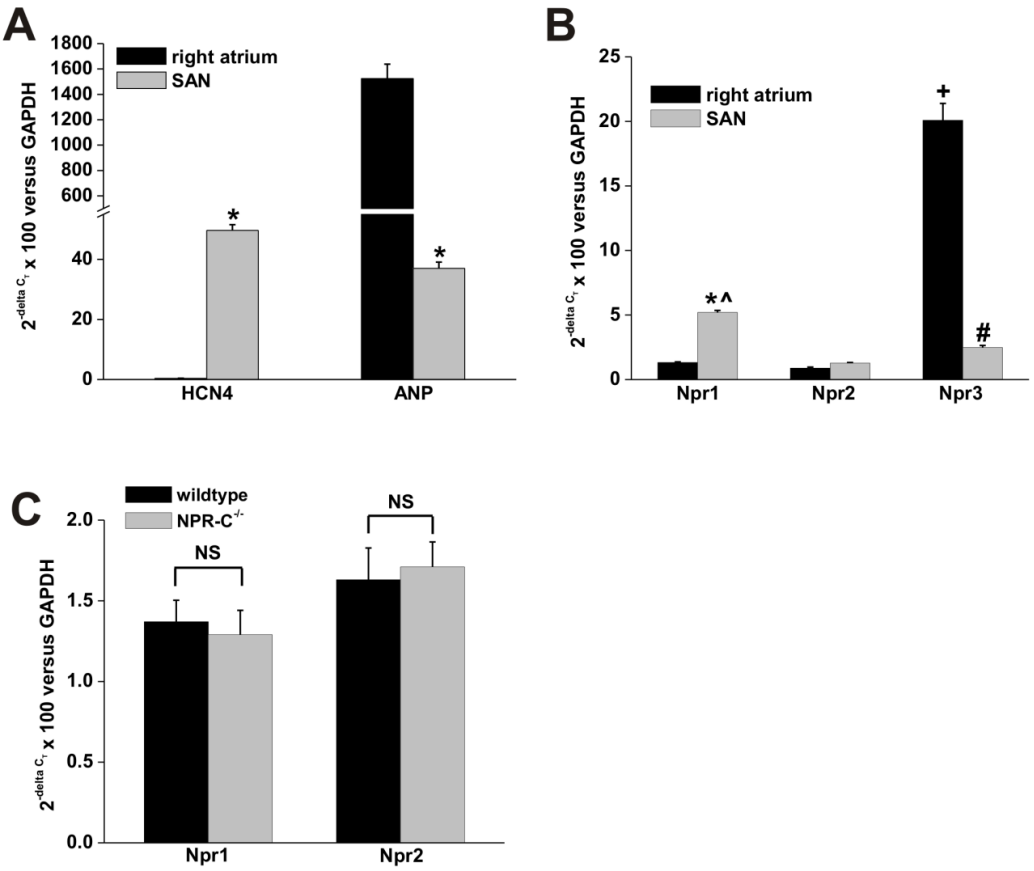

Supplemental Figure 1: Quantitative mRNA expression of natriuretic peptide receptors in SAN and right atrial myocardium. (A) Samples were confirmed to be from the SAN or right atrium by the characteristic pattern of expression of HCN4 and ANP in these regions. SAN tissue shows high expression of HCN4 and very low expression of ANP whereas the right atrium shows very low HCN4 expression and very high ANP expression. Note scale break on Y-axis. (B) Expression of Npr1, Npr2 and Npr3 mRNA (which correspond to NPR-A, NPR-B and NPR-C proteins respectively) relative to GAPDH. Each Npr mRNA was detected in SAN and right atrial tissue. Data are means ± SEM; n=5 trials, *P<0.05 vs. Npr2 within SAN samples. ^{+}P<0.001 vs. Npr1 and Npr2 within right atrial samples. ^P<0.05 vs. right atrium for Npr1. $^{\#}P$<0.001 vs. right atrium for Npr3. Data were analyzed using a two way ANOVA with Tukey's posthoc test. (C) Expression of Npr1 and Npr2 in whole right atrial samples (also containing the SAN) in wildtype and NPR-$C^{-/-}$ mice. Expression of Npr1 and Npr2 were not altered in mice lacking functional NPR-C receptors; n=3 trials.

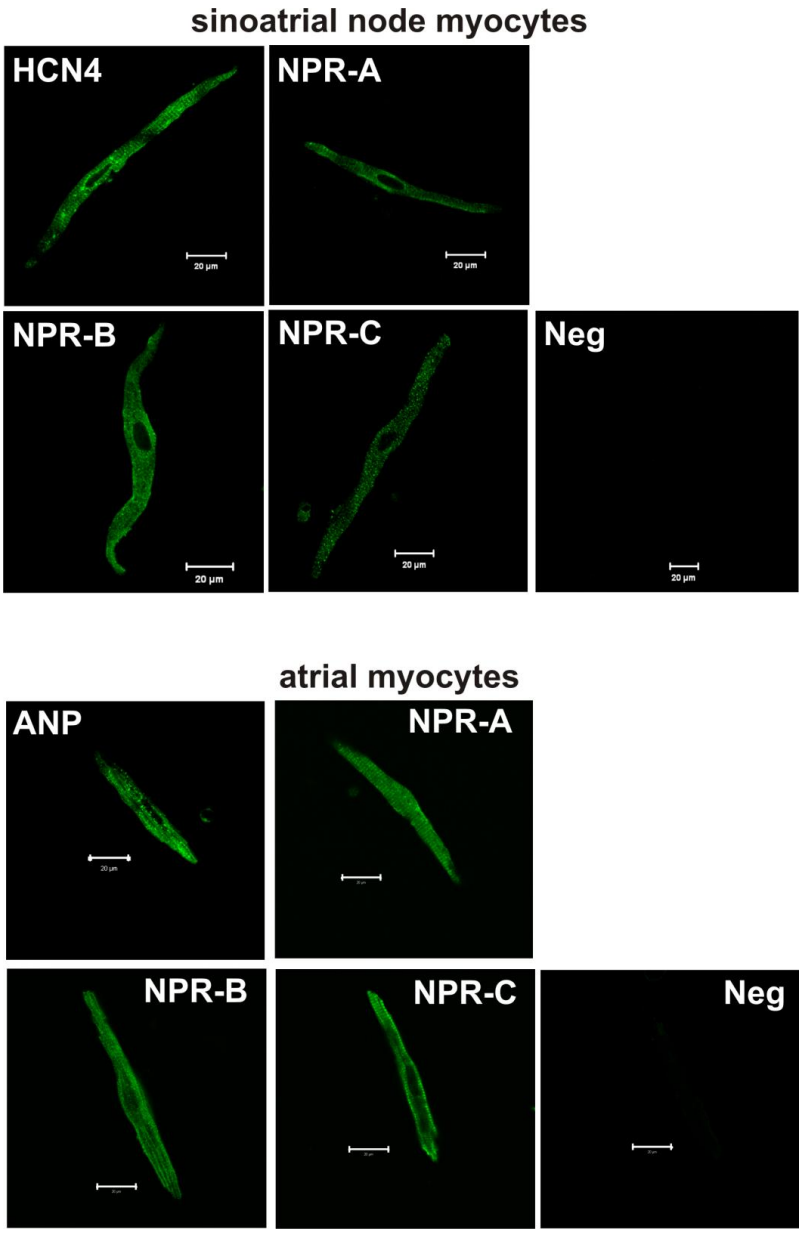

Supplemental Figure 2: Expression of natriuretic peptide receptor proteins in isolated SAN and right atrial myocytes. Spindle shaped SAN myocytes were isolated from the SAN region and shown to stain positively for HCN4 while working myocytes from the right atrial appendage stained positively for ANP. Groups of cells from the same isolations were then stained for NPR-A, NPR-B or NPR-C using specific antibodies. Omission of primary antibody (Neg) produced no non-specific staining. These data confirm that all three NPRs are expressed in SAN and atrial myocytes. Scale bars are 20 μM.

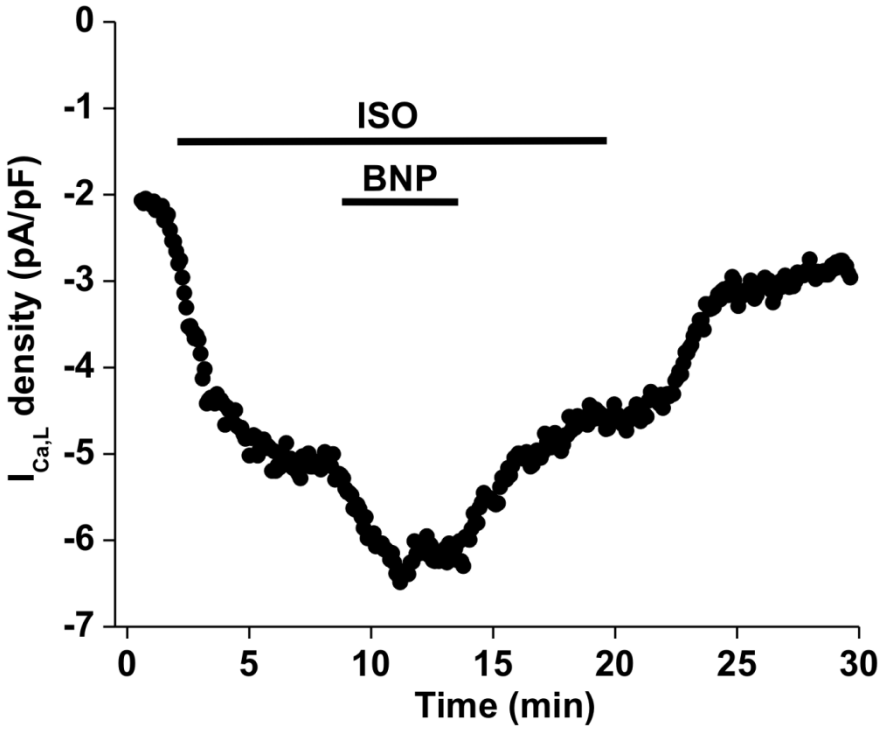

Supplemental Figure 3: Representative time course plot illustrating the effects of ISO and BNP on right atrial $I_{Ca,L}$ measured at 0 mV. ISO (10 nM) increased $I_{Ca,L}$ and subsequent application of BNP (100 nM) further augmented $I_{Ca,L}$. The effects of BNP and ISO were both reversible upon washout.

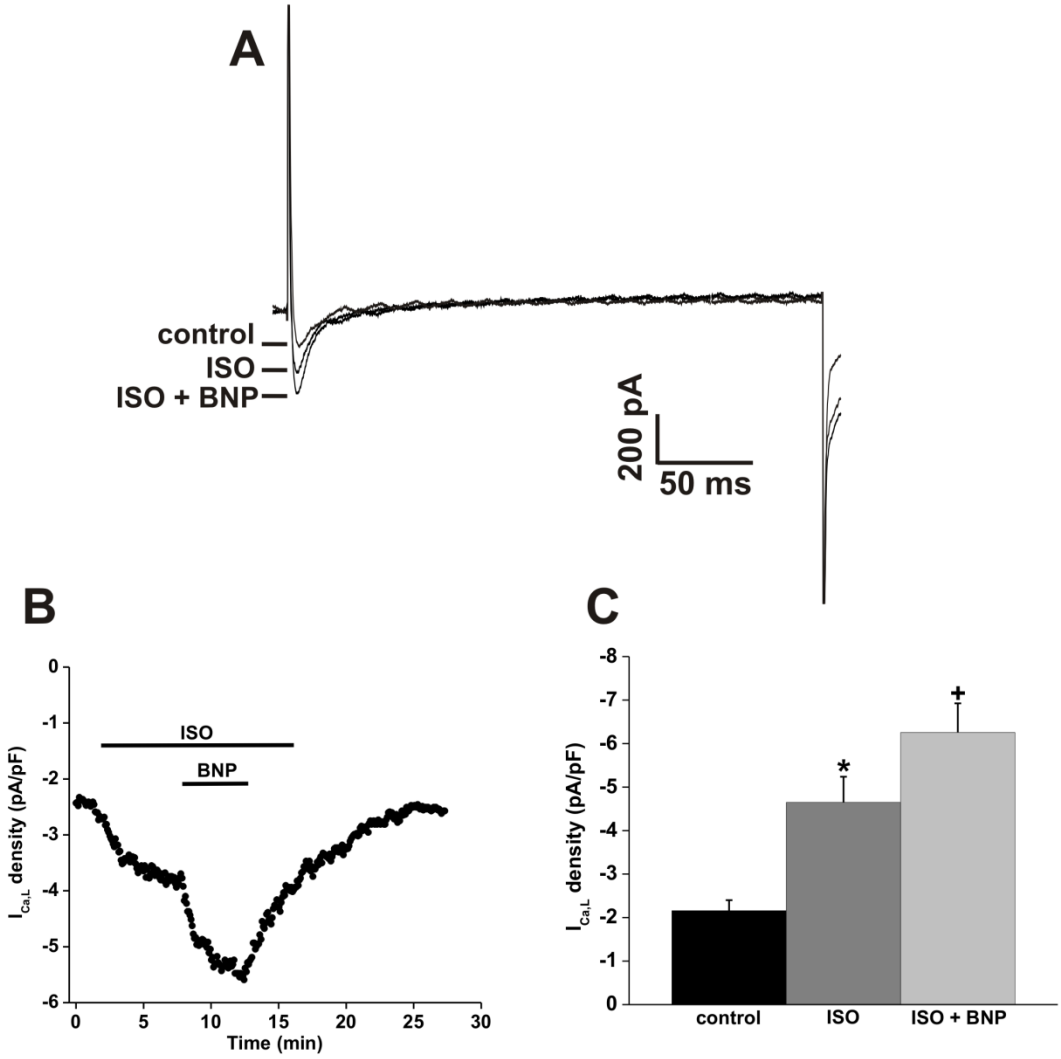

Supplemental Figure 4: Effects of BNP on $I_{Ca,L}$ in the presence of ISO in right atrial myocytes isolated from mutant mice lacking functional NPR-C receptors (NPR-$C^{-/-}$). (A) Representative $I_{Ca,L}$ recordings at 0 mV in right atrial myocytes from NPR-$C^{-/-}$ mice in control conditions, in the presence of ISO (10 nM), and after application of BNP (100 nM) in the presence of ISO. (B) Representative time course of the effects of ISO and BNP on $I_{Ca,L}$ in NPR-$C^{-/-}$ right atrial myocytes. (C) Summary of the effects of ISO and BNP on $I_{Ca,L}$ density at 0 mV in NPR-$C^{-/-}$ right atrial myocytes. Data are means ± SEM; *n*=8 myocytes; **P*<0.05 vs. control, $^{+}$*P*<0.05 vs. ISO by one way ANOVA with a Student-Newman-Keuls posthoc test. These data demonstrate that the ability of BNP to increase right atrial $I_{Ca,L}$ in the presence of ISO is not dependent on NPR-C.

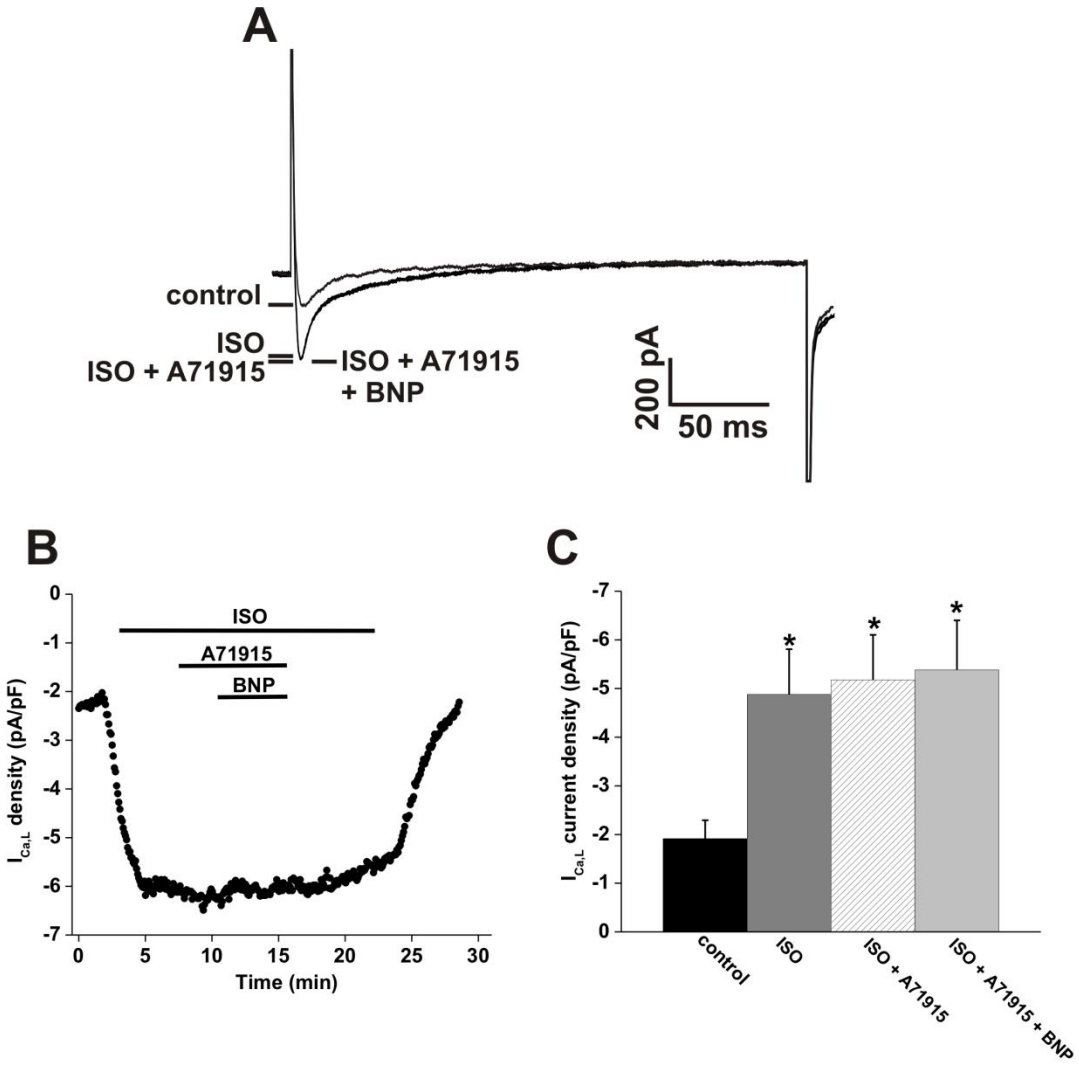

Supplemental Figure 5: Effects of BNP on $I_{Ca,L}$ in the presence of ISO in right atrial myocytes following NPR-A blockade with A71915. (A) Representative $I_{Ca,L}$ recordings at 0 mV in right atrial myocytes in control conditions, in the presence of ISO (10 nM), in the presence of ISO and A71915 (500 nM) and after application of BNP (100 nM) in the presence of ISO and A71915. (B) Representative time course of the effects of ISO, A71915 and BNP on $I_{Ca,L}$ in right atrial myocytes. (C) Summary of the effects of ISO, A71915 and BNP on $I_{Ca,L}$ density at 0 mV in right atrial myocytes. Data are means ± SEM; *n*=8 myocytes; **P*<0.05 vs. control by one way ANOVA with a Student-Newman-Keuls posthoc test. These data demonstrate that the effect of BNP on ISO stimulated atrial $I_{Ca,L}$ is completely antagonized by A71915 suggesting BNP elicits its effect by activating NPR-A.

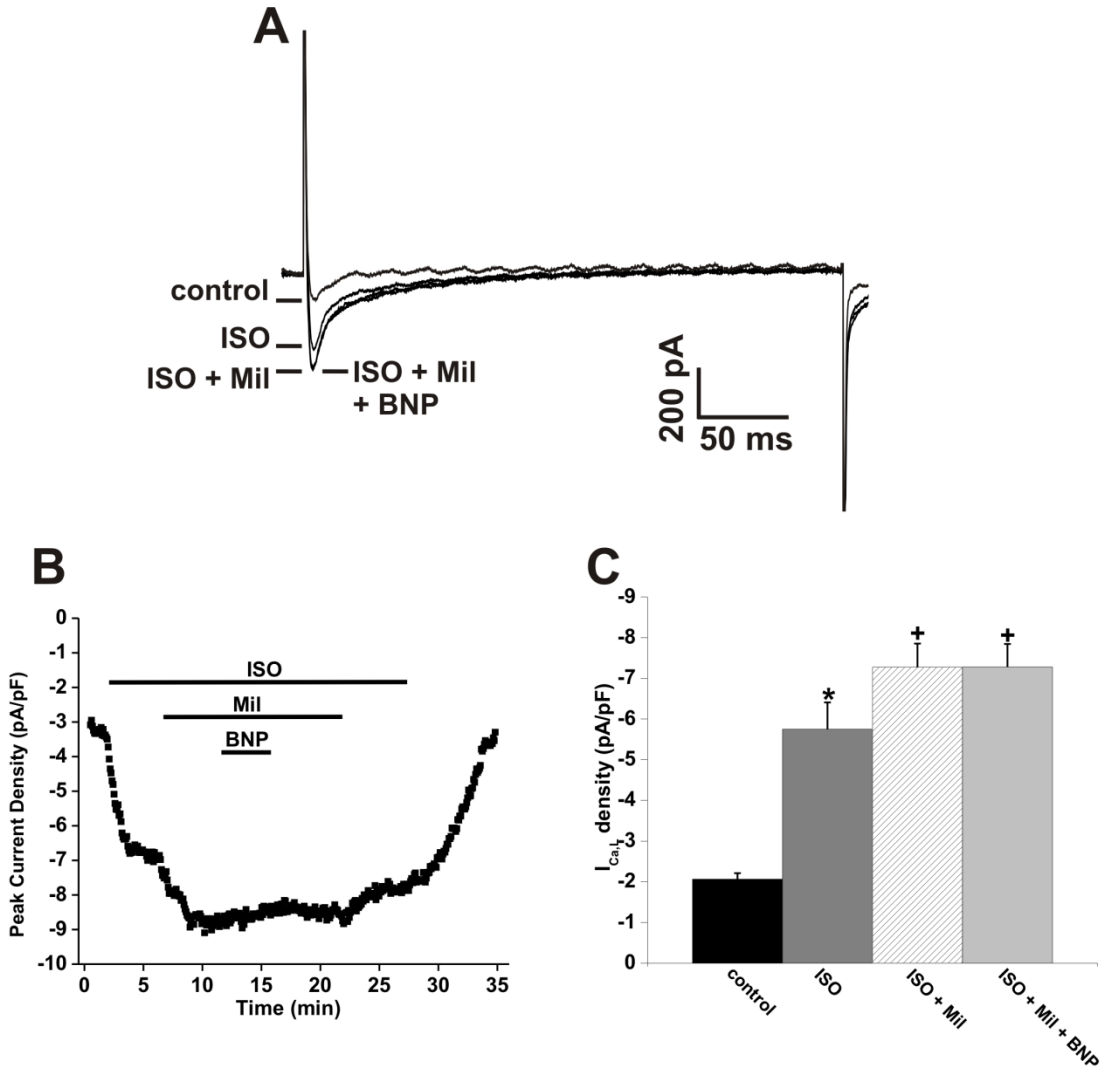

Supplemental Figure 6: Effects of BNP on $I_{Ca,L}$ in the presence of ISO in right atrial myocytes following blockade of phosphodiesterase 3 with milrinone. (A) Representative $I_{Ca,L}$ recordings at 0 mV in right atrial myocytes in control conditions, in the presence of ISO (10 nM), in the presence of ISO and Mil (10 μM) and after application of BNP (100 nM) in the presence of ISO and Mil. (B) Representative time course of the effects of ISO, Mil and BNP on $I_{Ca,L}$ in right atrial myocytes. (C) Summary of the effects of ISO, Mil and BNP on $I_{Ca,L}$ density at 0 mV in right atrial myocytes. Data are means ± SEM; *n*=7 myocytes; **P*<0.05 vs. control, $^{+}$*P*<0.05 vs. ISO by one way ANOVA with a Student-Newman-Keuls posthoc test. These data demonstrate that Mil increases ISO stimulated atrial $I_{Ca,L}$ to a similar extent as BNP and that BNP no longer has any effect $I_{Ca,L}$ following PDE3 blockade.

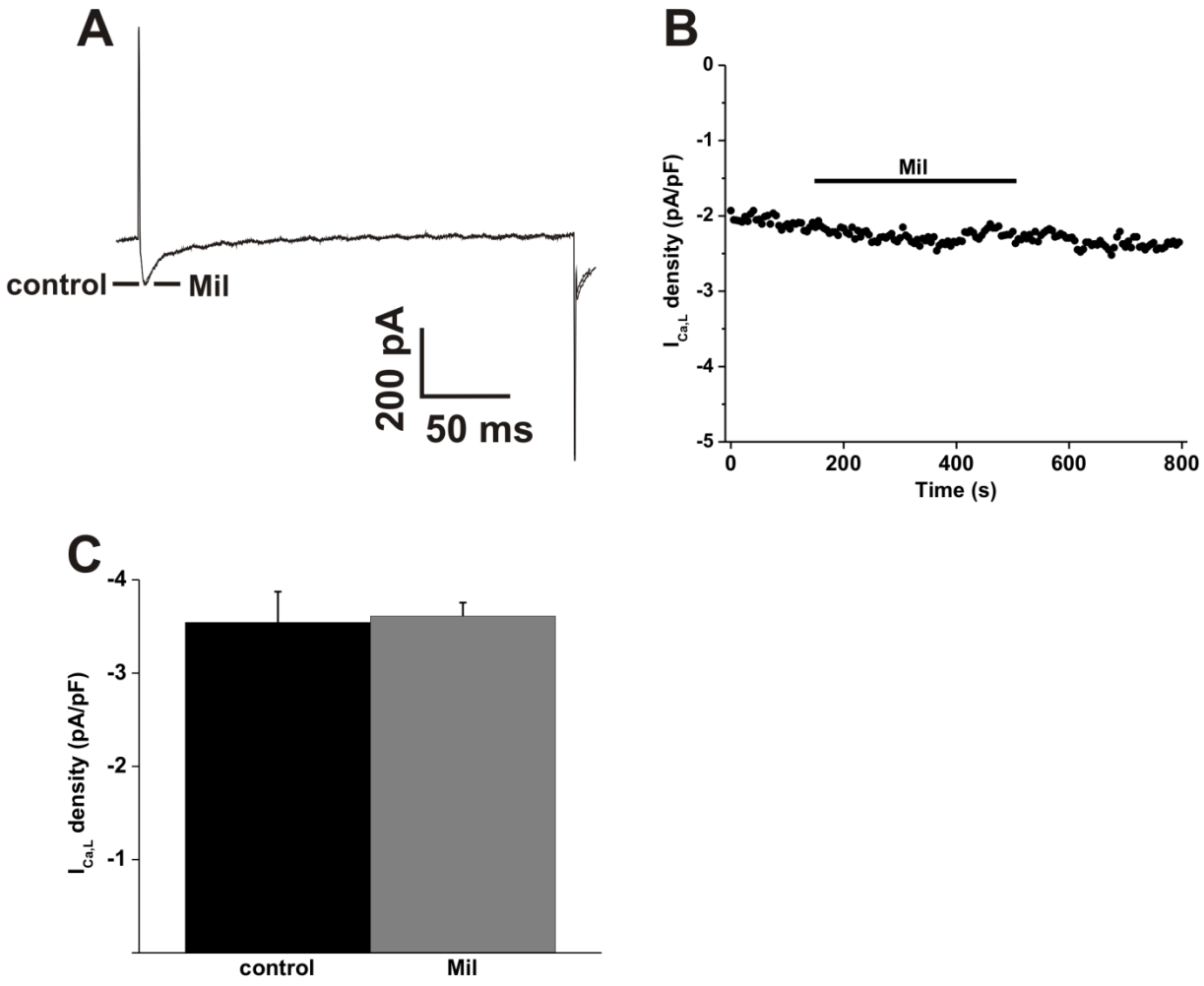

Supplemental Figure 7: Effects of the phosphodiesterase 3 inhibitor milrinone on right atrial $I_{Ca,L}$ in basal conditions. (A) Representative $I_{Ca,L}$ recordings at 0 mV in right atrial myocytes in control conditions and in the presence of Mil (10 µM). (B) Representative time course of the effects of Mil on $I_{Ca,L}$ in right atrial myocytes. (C) Summary of the effects of Mil on $I_{Ca,L}$ density at 0 mV in right atrial myocytes. Data are means ± SEM; *n*=12 myocytes. Mil had no significant effect on right atrial $I_{Ca,L}$ in basal conditions.

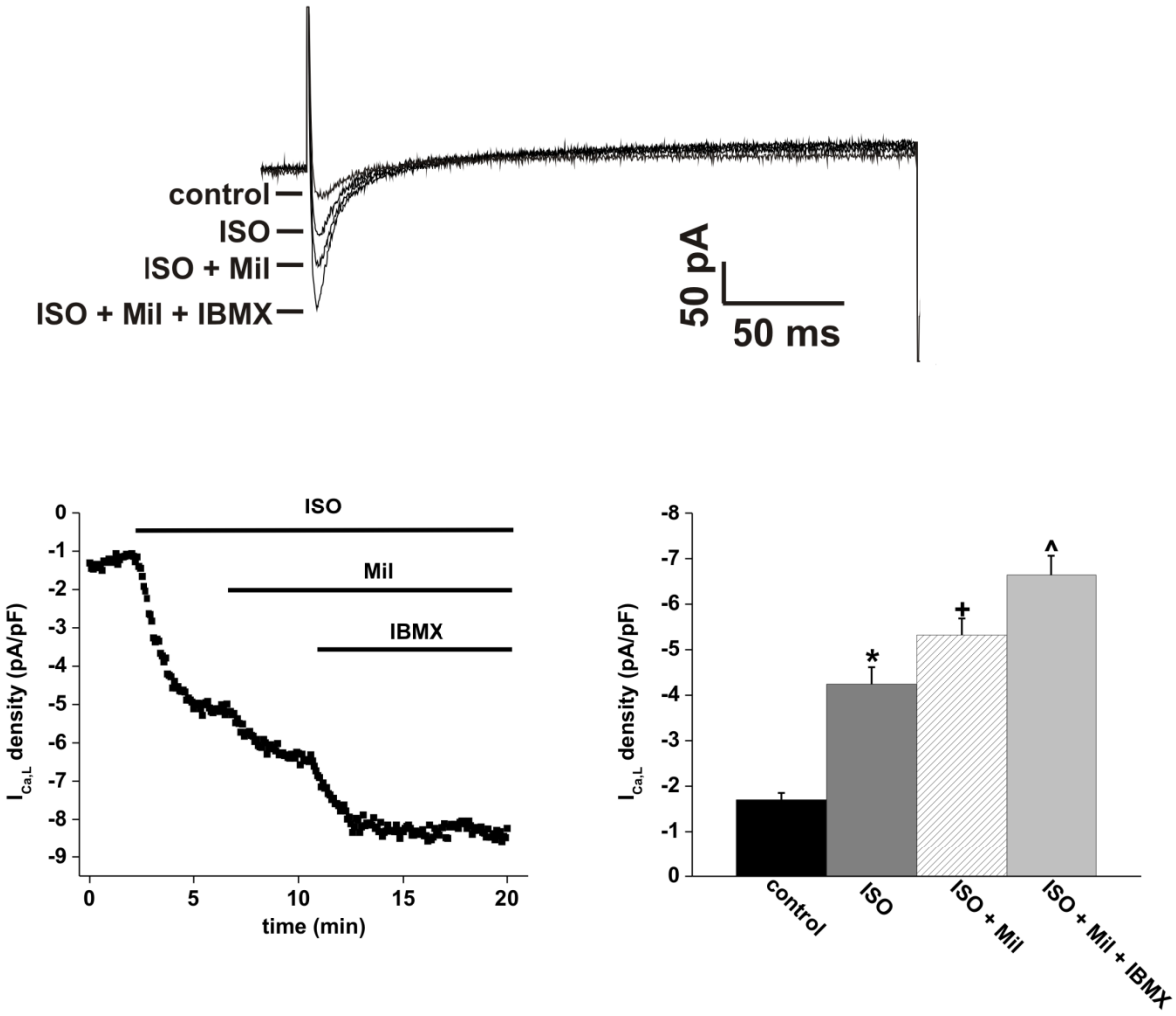

Supplemental Figure 8: Effects of the broad spectrum PDE inhibitor IBMX on right atrial $I_{Ca,L}$ in the presence of ISO and milrinone. (A) Representative $I_{Ca,L}$ recordings at 0 mV in control conditions, in the presence of ISO (10 nM), in ISO and Mil (10 µM) and in the presence of ISO, Mil and IBMX (50 µM). (B) Representative time course of the effects of ISO, Mil and IBMX on right atrial $I_{Ca,L}$. (C) Summary of the effects of ISO, Mil and IBMX on right atrial $I_{Ca,L}$ density at 0 mV. Data are means ± SEM; *n*=7 myocytes; **P*<0.05 vs. control, $^{+}$*P*<0.05 vs. ISO, ^*P*<0.05 vs. ISO + Mil by one way ANOVA with a Tukey posthoc test. These data demonstrate that IBMX can further increase atrial $I_{Ca,L}$ following the application of ISO and Mil.

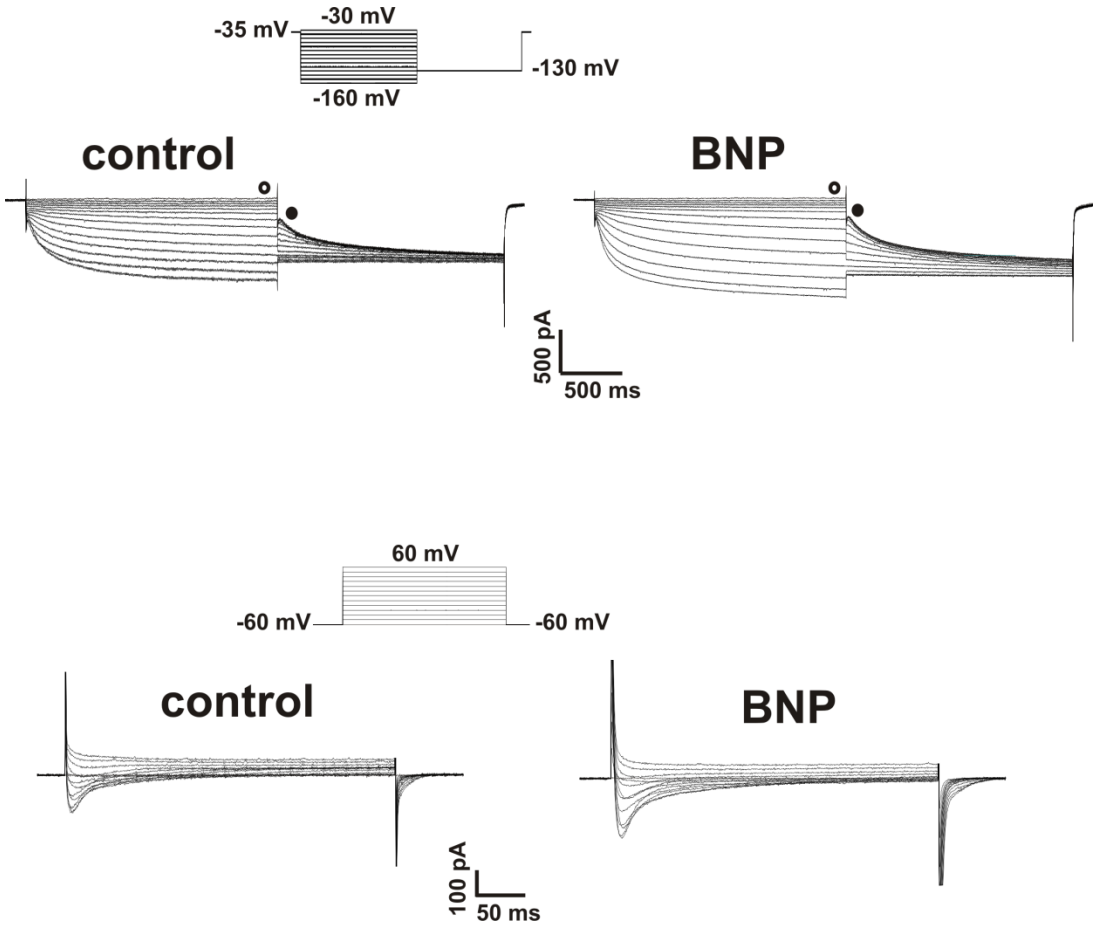

Supplemental Figure 9: Representative examples of I_f (top) and $I_{Ca,L}$ (bottom) recordings used to generate full current-voltage (I-V) relationships and to analyze activation kinetics. For the I_f recordings (top) the open circle indicates the time point used to generate I-V relationships and the filled circle indicates the time point used to analyze activation kinetics. These examples illustrate recordings in control conditions and following the application of BNP (100 nM) in isolated SAN myocytes.

References

[1] Jaubert J, Jaubert F, Martin N, Washburn LL, Lee BK, Eicher EM, et al. Three new allelic mouse mutations that cause skeletal overgrowth involve the natriuretic peptide receptor C gene (Npr3). Proc Natl Acad Sci U S A 1999;96:10278-83.

[2] Cifelli C, Rose RA, Zhang H, Voigtlaender-Bolz J, Bolz SS, Backx PH, et al. RGS4 Regulates Parasympathetic Signaling and Heart Rate Control in the Sinoatrial Node. Circ Res 2008;103:527-35.

[3] Lomax AE, Rose RA, Giles WR. Electrophysiological evidence for a gradient of G protein-gated K^+ current in adult mouse atria. Br J Pharmacol 2003;140:576-84.

[4] Mangoni ME, Nargeot J. Properties of the hyperpolarization-activated current (I_f) in isolated mouse sino-atrial cells. Cardiovasc Res 2001;52:51-64.

[5] Rose RA, Lomax AE, Kondo CS, Anand-Srivastava MB, Giles WR. Effects of C-type natriuretic peptide on ionic currents in mouse sinoatrial node: a role for the NPR-C receptor. Am J Physiol 2004;286:H1970-H1977.

[6] Rose RA, Kabir MG, Backx PH. Altered heart rate and sinoatrial node function in mice lacking the cAMP regulator phosphoinositide 3-kinase-gamma. Circ Res 2007;101:1274-82.

[7] Rae J, Cooper K, Gates P, Watsky M. Low access resistance perforated patch recordings using amphotericin B. J Neurosci Methods 1991;37:15-26.

[8] Hamill OP, Marty A, Neher E, Sakmann B, Sigworth FJ. Improved patch-clamp techniques for high-resolution current recording from cells and cell-free membrane patches. Pflugers Arch 1981;391:85-100.

[9] Mangoni ME, Couette B, Bourinet E, Platzer J, Reimer D, Striessnig J, et al. Functional role of L-type Cav1.3 Ca^{2+} channels in cardiac pacemaker activity. Proc Natl Acad Sci U S A 2003;100:5543-8.

[10] Zhang Z, Xu Y, Song H, Rodriguez J, Tuteja D, Namkung Y, et al. Functional Roles of $Ca_v1.3$ ($alpha_{1D}$) calcium channel in sinoatrial nodes: insight gained using gene-targeted null mutant mice. Circ Res 2002;90:981-7.

[11] Zhang Z, He Y, Tuteja D, Xu D, Timofeyev V, Zhang Q, et al. Functional roles of Cav1.3(alpha1D) calcium channels in atria: insights gained from gene-targeted null mutant mice. Circulation 2005;112:1936-44.

[12] Honjo H, Boyett MR, Kodama I, Toyama J. Correlation between electrical activity and the size of rabbit sino-atrial node cells. J Physiol 1996;496 (Pt 3):795-808.

[13] Rose RA, Sellan M, Simpson JA, Izaddoustdar F, Cifelli C, Panama BK, et al. Iron Overload Decreases CaV1.3-Dependent L-Type Ca2+ Currents Leading to Bradycardia, Altered Electrical Conduction, and Atrial Fibrillation. Circ Arrhythm Electrophysiol 2011;4:733-42.

[14] Denyer JC, Brown HF. Rabbit sino-atrial node cells: isolation and electrophysiological properties. J Physiol 1990;428:405-24.

[15] Gao Z, Chen B, Joiner ML, Wu Y, Guan X, Koval OM, et al. I_f and SR Ca^{2+} release both contribute to pacemaker activity in canine sinoatrial node cells. J Mol Cell Cardiol 2010;49:33-40.

[16] Marionneau C, Couette B, Liu J, Li H, Mangoni ME, Nargeot J, et al. Specific pattern of ionic channel gene expression associated with pacemaker activity in the mouse heart. J Physiol 2005;562:223-34.

[17] Liu J, Dobrzynski H, Yanni J, Boyett MR, Lei M. Organisation of the mouse sinoatrial node: structure and expression of HCN channels. Cardiovasc Res 2007;73:729-38.